Enhanced Large-Scale Modeling of Additive Manufacturing: Layer-wise Equivalent Heat Flux Attribution for Thermal Interaction Analysis across Multiple Fabrications

Fan Chen, Dominik Kozjek, Conor Porter, Jian Cao

Email: fanchen@northwestern.edu

Supervisor: Jian Cao

March 24, 2025

Background

Metal additive manufacturing (AM) process:
- Laser powder bed fusion
- Directed energy deposition

Temperature history determines:
- Residual stress
- Fluid dynamics
- Microstructure evolution
- Part distortion
- Defects
- Mechanical properties

High-fidelity coupled CFD-FEM modeling

CFD

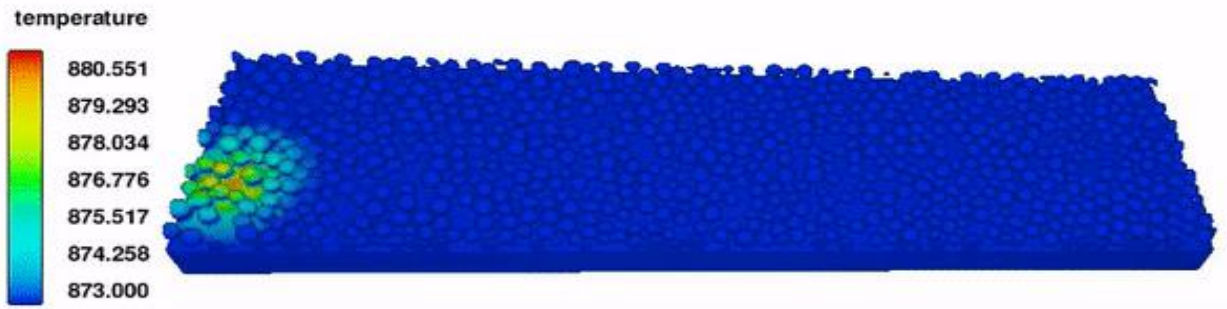

Coupled CFD-FEM

Two-layer two-track: high computational cost

Chen F, Yan W. Materials & Design, 2020, 196: 109185.

Large-scale FEM approaches in AM (1/2)

- Track-by-track heating + agglomeration

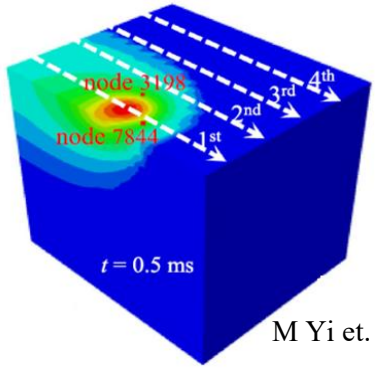

M Yi et. al. [1]

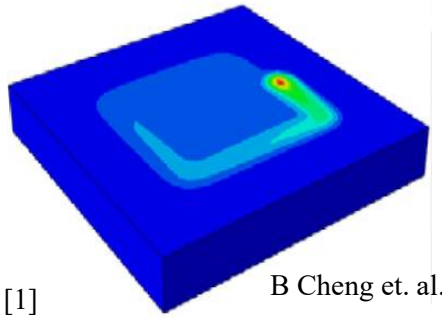

B Cheng et. al. [2]

- Equivalent strain/temperature attribution [3,4] + element activation

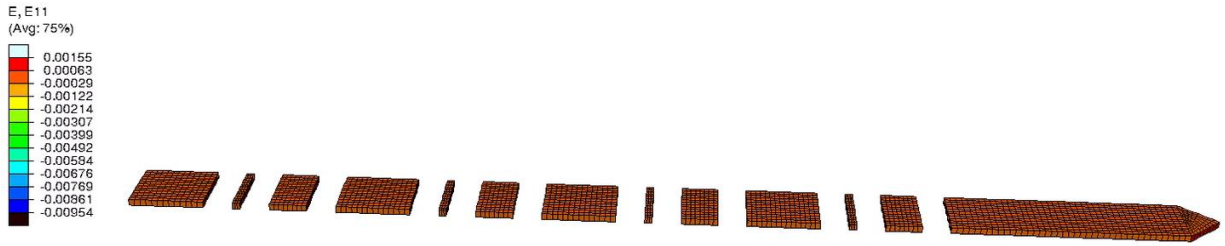

- Temperature
- Strain tensor

→ Equivalent layer →

- Cooling
- Relaxation

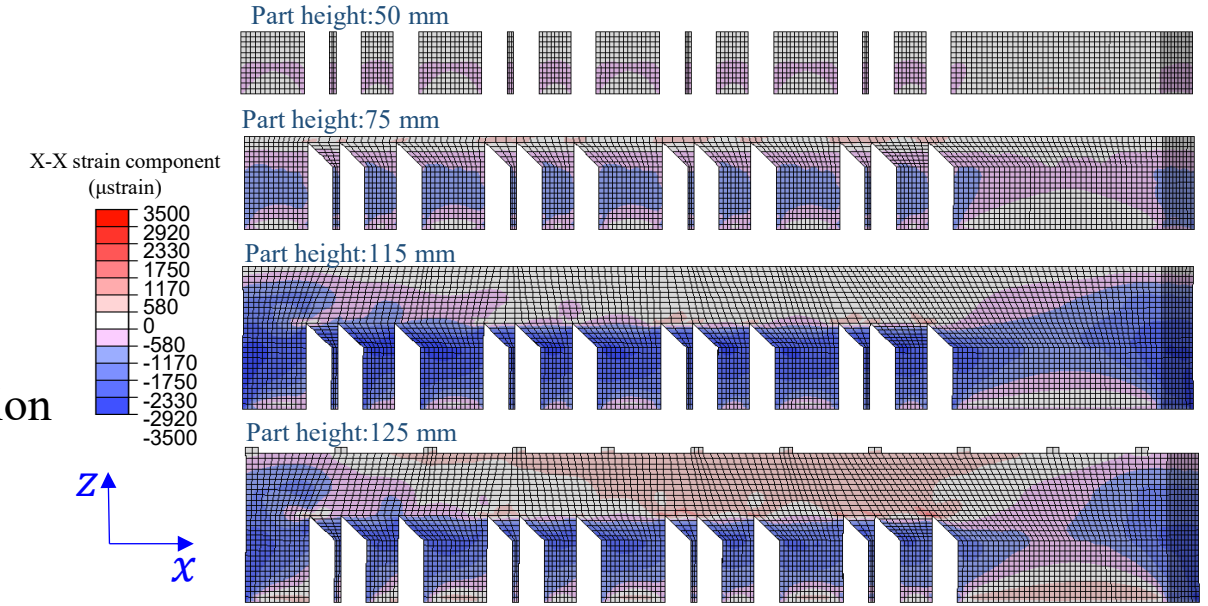

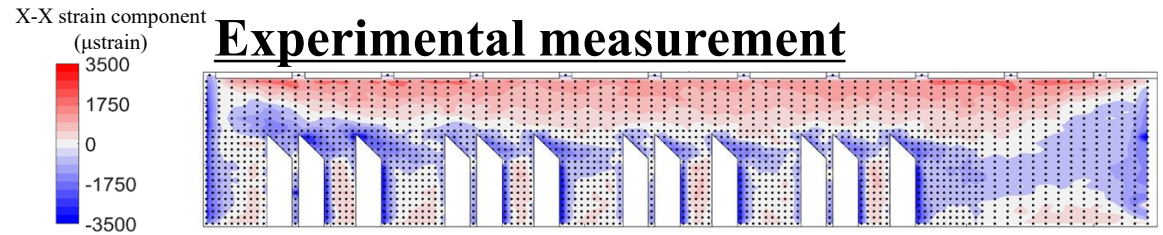

Accurate inherent strain pattern + Neutralization

[11 Yi M, Xu B X, Gutfleisch O. Computational Mechanics, 2019, 64(4): 917-935.
[2] Cheng B, Shrestha S, Chou K. Additive Manufacturing, 2016, 12: 240-251.
[3] Olleak A, Xi Z. Manufacturing Letters, 2020, 24: 140-144.
[4] Liang, X., Chen, Q., Cheng, L., Hayduke, D., & Albert C. To (2019). *Computational Mechanics*, *64*, 1719-1733.

Large-scale FEM approaches in AM (2/2)

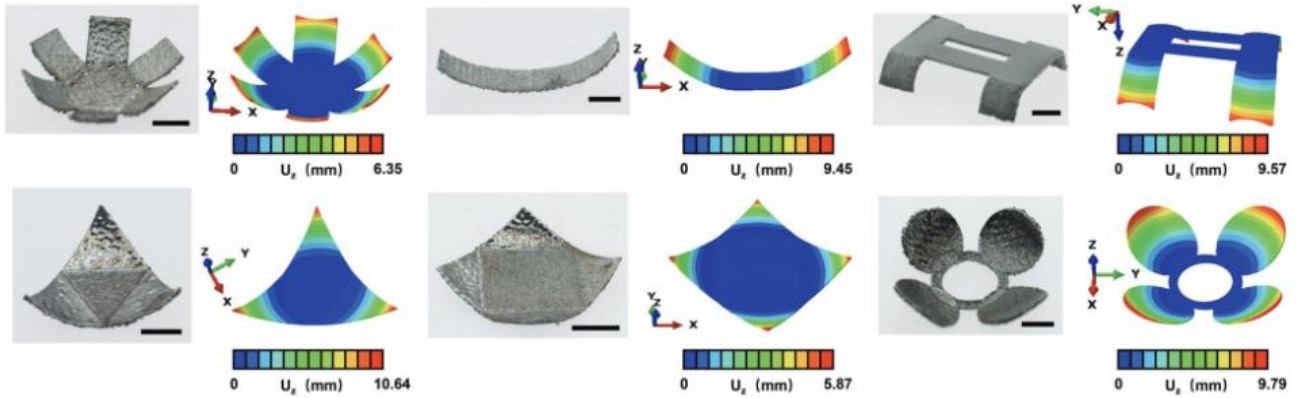

(Selected as the cover of "*Advanced Science 12/ 2023*" Wu, W. et al)

Heating step
- Temperature
- Heat flux

Cooling step
- Radiation
- Convection

Layer refresh

Metallic 4D Printing of Laser Stimulation (Adv. Sci. 12/2023)

Wenzheng Wu, Yiming Zhou, Qingping Liu, Luquan Ren, Fan Chen, Jerry Ying Hsi Fuh, Aodu Zheng, Xuechao Li, Ji Zhao, Guiwei Li

2370067 | First Published: 26 April 2023

4D Printing

In article number 2206486 by Guiwei Li and co-workers, a 4D printing method to endow non-shapememory metallic materials with active properties is presented, which can realize the shape changing of selected areas during or after forming process owing to stress release generated. The methodology opens new avenues to create metallic shape-morphing 3D structures for high-performance engineering applications. Specifically, the 2D part precursor can be turned into fitting a 3D structure by laser stimulation to repair the gap of the space station.

Distortion and residual stress can be accurately predicted by:
the reasonable configurations of the equivalent **stress, strain, heat flux or temperature** attribution.

[1] Wu, W., Zhou, Y., Liu, Q., Ren, L., **Fan, C.**, Fuh, J. Y. H., ... & Li, G. (2023). *Advanced Science*, *10*(12), 2206486.
[2] Alvarez P, Ecenarro J, Setien I, et al. Int. J. Eng. Res. Sci, 2016, 2(10): 39-46.

Problems

Individual specimens

(Dominik and Conor)

Single part simulation

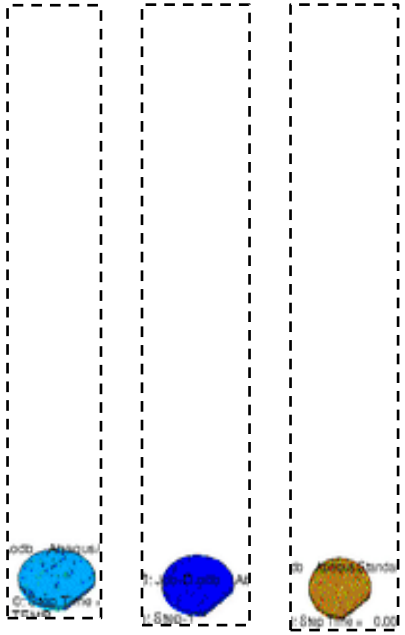

Advantages:

- Easy implementation
- Good efficiency

Problems

- Material deposition
- Heat source
- Thermal boundary

(Kozjek et al.)

Multiple parts:

- Geometry feature
- Scan pattern
- Interlayer heat variation

Fabrication design → Assumptions & Simplifications: → Temperature field prediction

Kozjek, D., Porter, C., Carter III, F. M., Mogonye, J. E., & Cao, J. (2023). *Journal of Manufacturing Processes*.

Objective of this research

Specimen **cluster**

(Dominik and Conor)

Whole build:

1633 layers
×
67 tracks
=
107 millions of tracks

Multiple specimens simulation:

- Reasonable **thermal boundary**;
- Incorporation of **scan pattern**;
- Easy implementation;
- Good accuracy.

Kozjek, D., Porter, C., Carter III, F. M., Mogonye, J. E., & Cao, J. (2023). *Journal of Manufacturing Processes*.

Proposed modeling framework

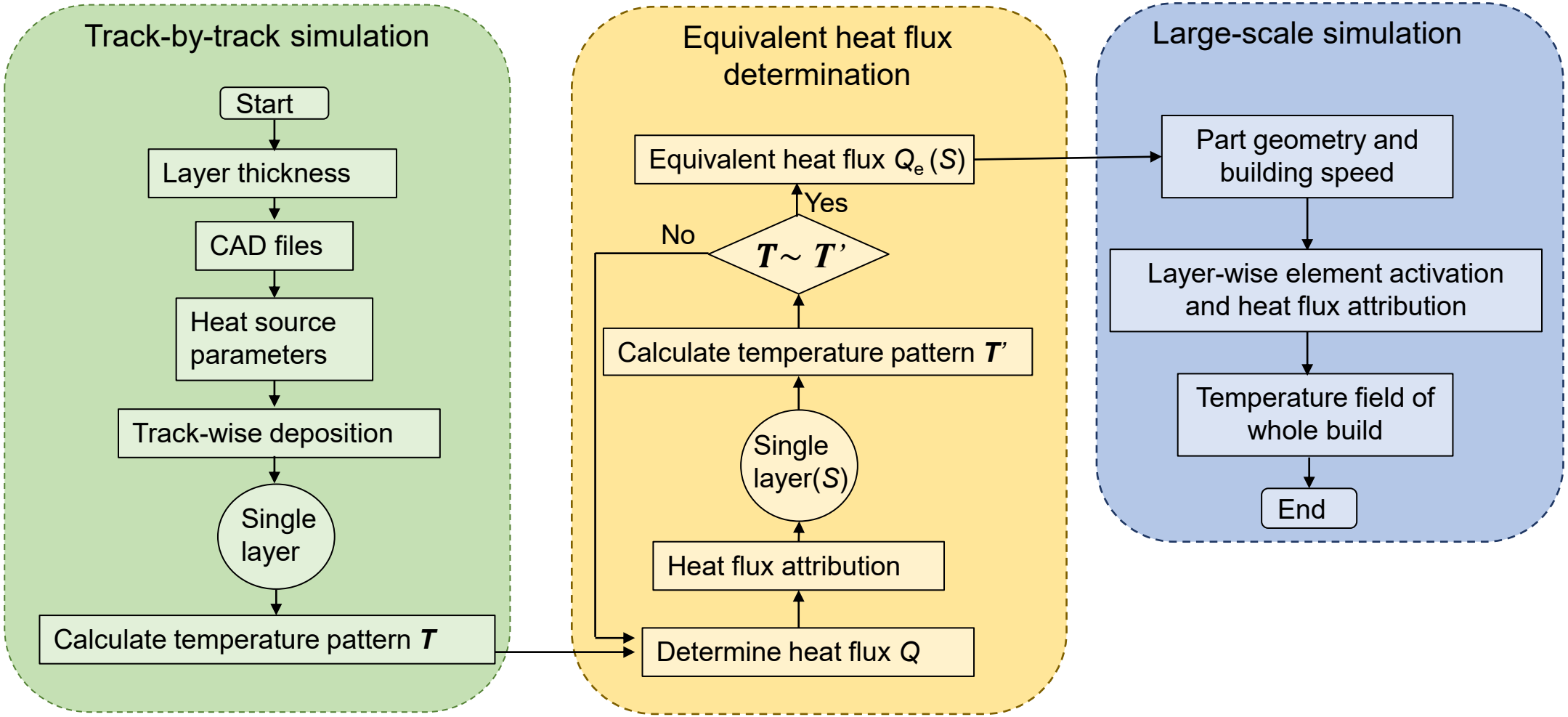

Proposed modeling framework

Model 1: Track-by-track heating

Model 2: layer-wise heat flux attribution

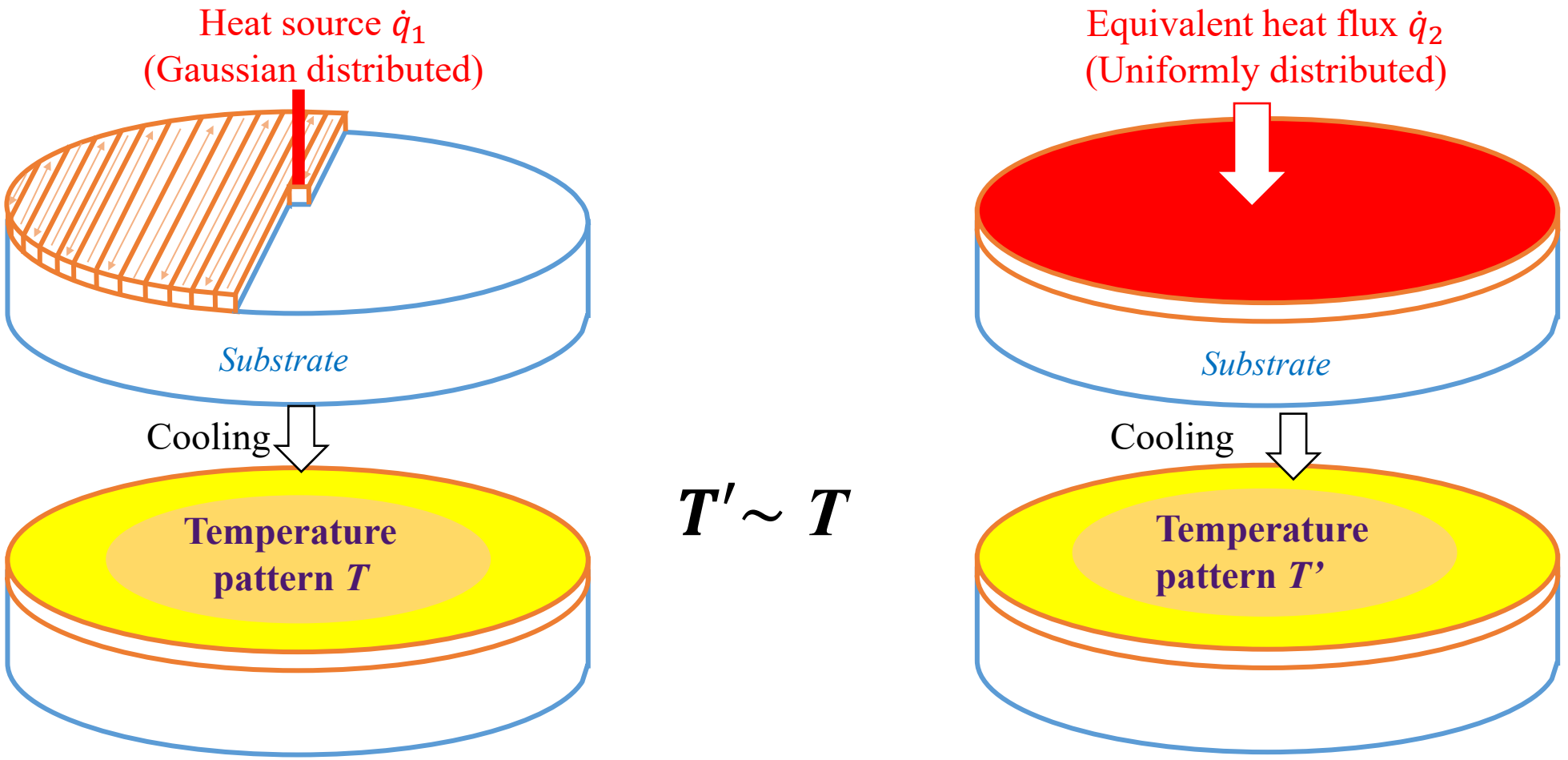

Governing equations

- Energy balance

$$\int_V \rho \dot{U} dV = \int_S q dS + \int_V r dV$$

V: volume of solid material (m^3)
S: surface area (m^2)
ρ: density of the material (kg/m^3)
$\dot{U}$: material time rate of internal energy (W/kg)
q: heat flux per unit area, flow into body (W/m^2)
r: heat supplied externally into the body (W/m^3)

- Constitutive definition

In terms of specific heat: $c(\theta) = \frac{dU}{d\theta}$

Heat conduction by Fourier law: $\boldsymbol{f} = -\boldsymbol{k}\frac{\partial \theta}{\partial x}$

- Surface heat flux

Track-by-track scanning: $\dot{q}_1 = \frac{Q}{\pi r_0^2} exp\left(1 - \frac{r^2}{r_0^2}\right)$

Uniform distribution: $\dot{q}_2 = Q_e$

- Radiation

$$\dot{q}_2 = A((\theta - \theta^Z)^4 - (\theta^0 - \theta^Z)^4)$$

A: radiation constant ($W/(m^2 \cdot K^4)$)
θ^0: sink temperature (K)
θ^Z: absolute zero on temperature scale (K)

- Surface convection

$$q = h(\theta - \theta^0)$$

h: film coefficient ($W/(m^2 \cdot K)$)

Circular shape

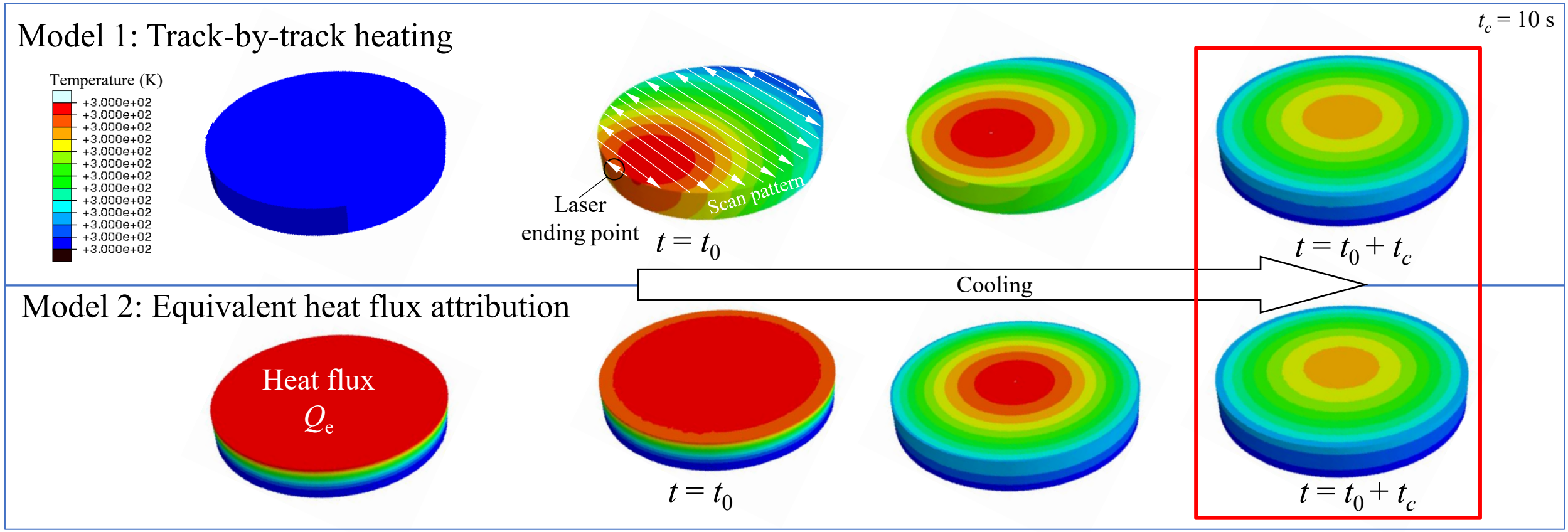

Rectangular shape

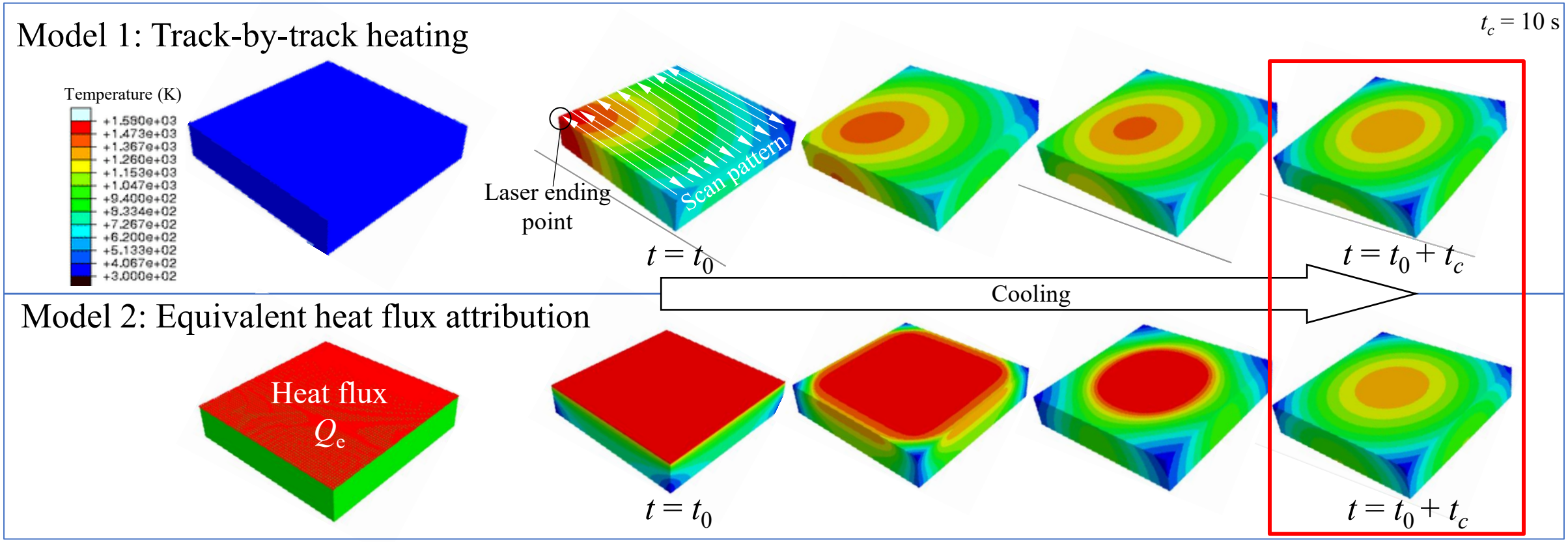

If Q_e is properly selected:

The two different heating method obtain the **similar temperature pattern** after the cooling time t_c.
(under the same thermal boundary conditions)

Heat transfer analysis on a single layer

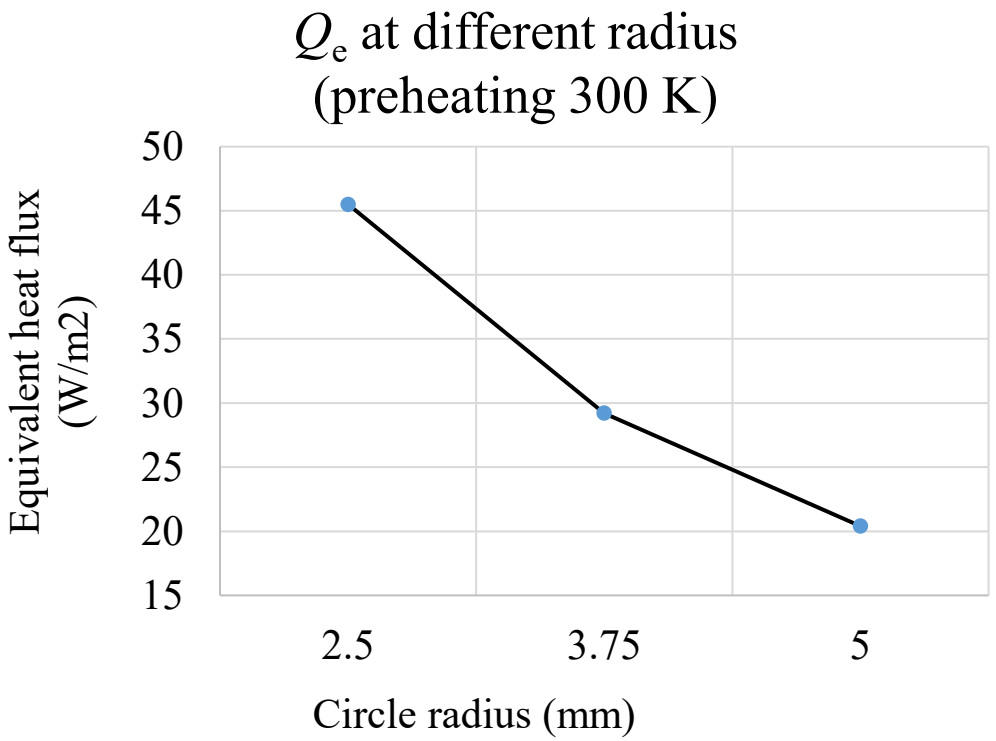

Q_e at preheating temperature (circular radius 3.75 mm)

Preheating (K)	Q_e (W/m^2)	Temperature after cooling (K)	Residual temperature with Q_e=29.2 W/m^2
300	29.2 - 29.3	785.6	785.6
500	28.2 - 28.3	802.7	803.2
700	27.8 - 27.9	856.5	857.1

Residual temperature: the preheating for the next layer

Heat transfer analysis on a single layer

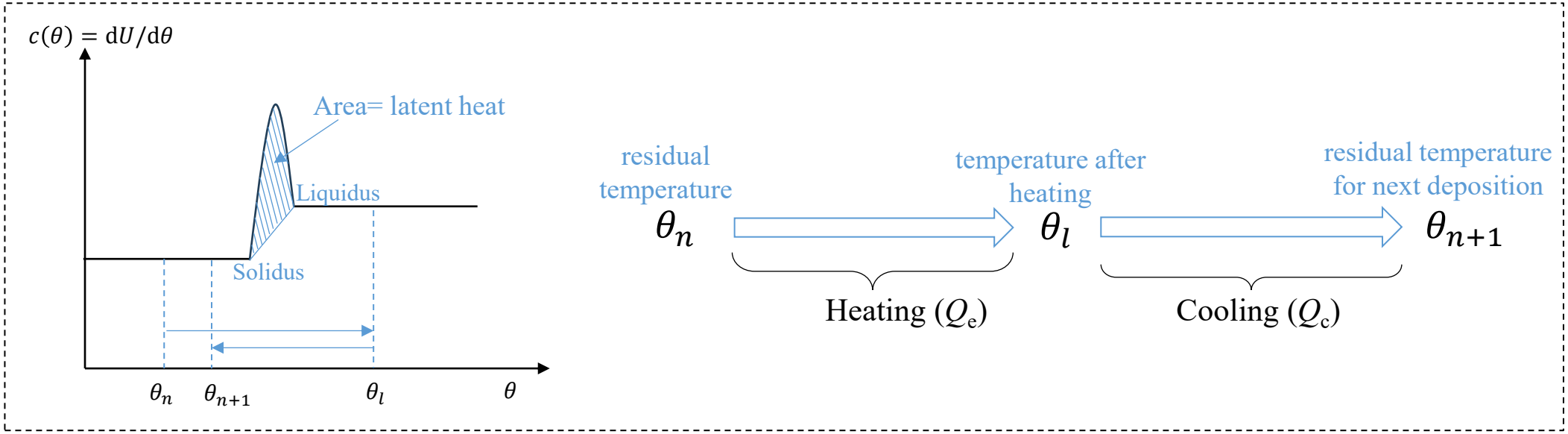

Temperature change:

$$\Delta\theta = \frac{U}{cm}$$

(Rough estimation)

U: energy
c: specific heat
m: mass

Assumption:

To make the similar $\Delta\theta$, Q_e is primarily depending on

- **laser parameters**
- **cross section area *S***

Part-scale heat flux attribution

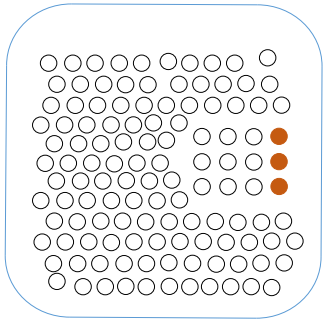

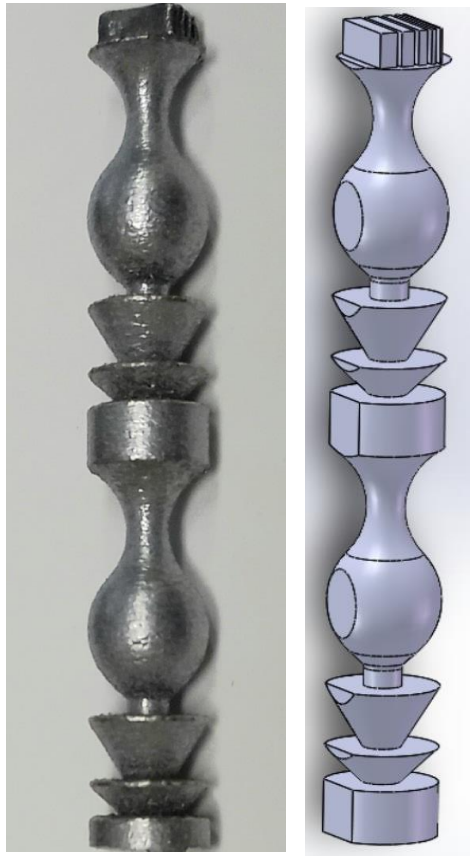

- Thermal load

Track-by-track heating

Uniform distributed heat flux

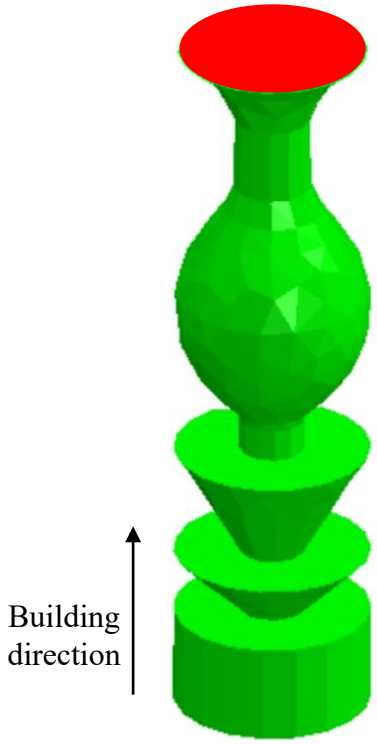

- Thermal boundary condition

LPBF:

Thermal conduction of the **powder particles cannot be simplified as** radiation and convection

Computational cost (per layer): 2~3 CPU hours Within 1 min

Model geometry of the specimen clusters

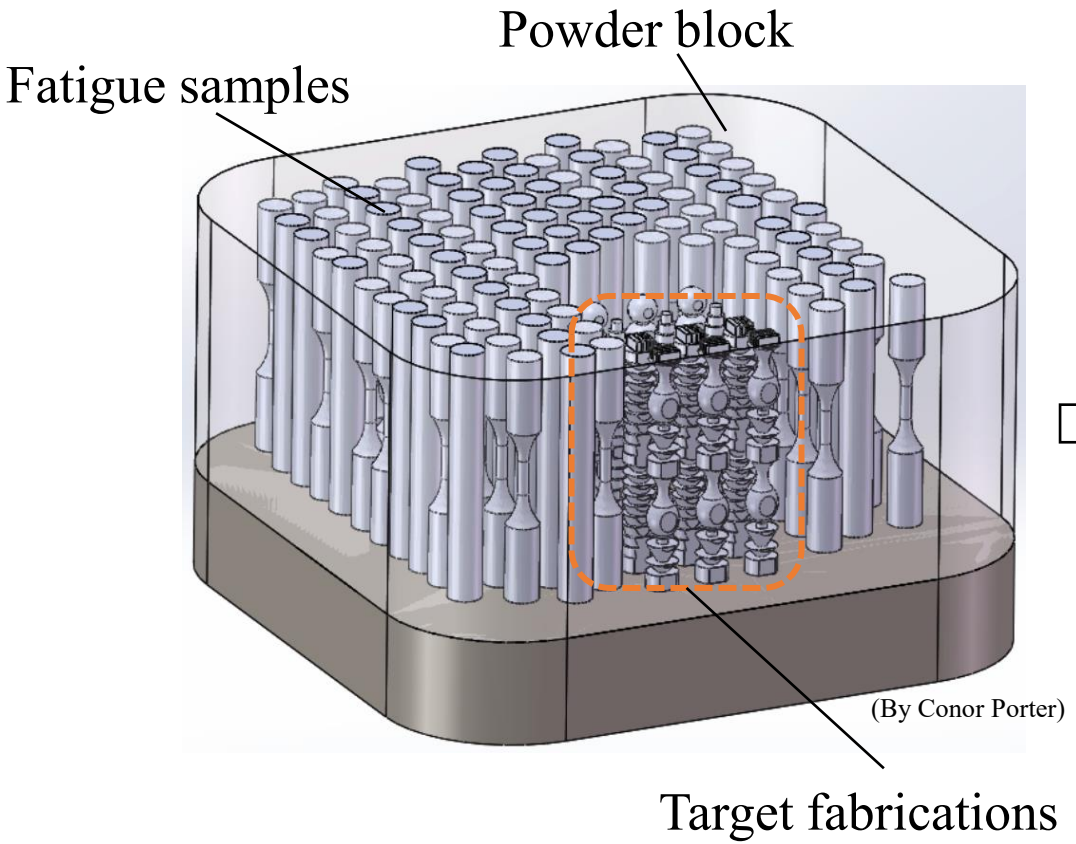

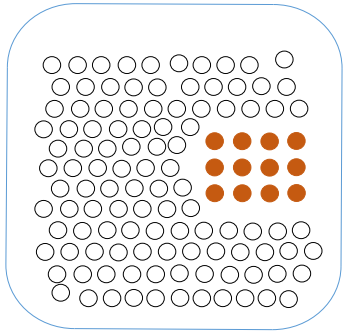

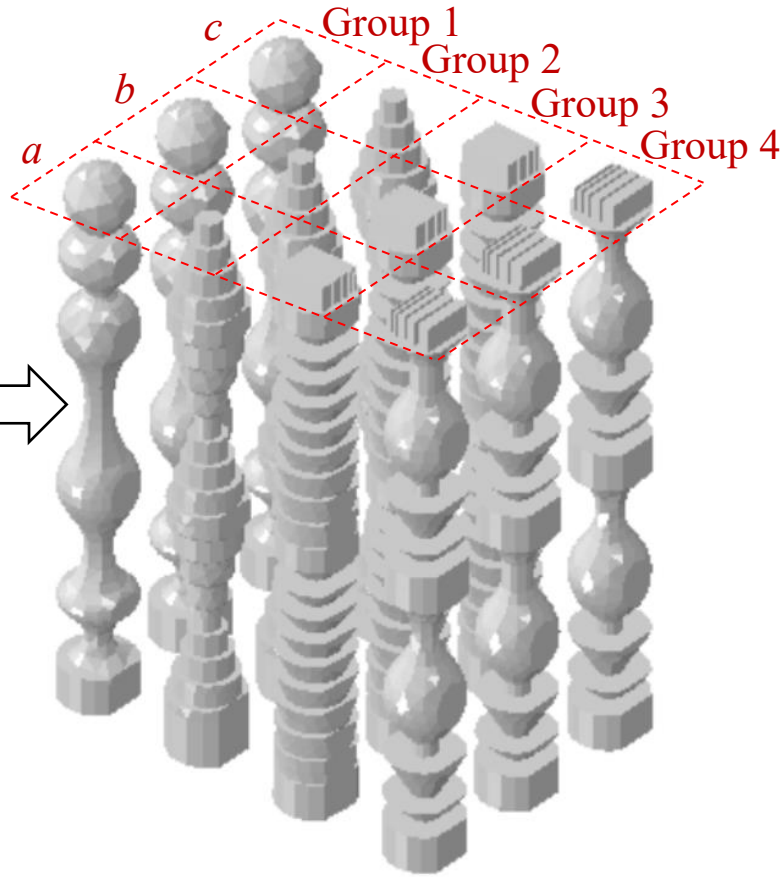

Model construction

Track-scale simulation:

- scan speed: 1550 mm/s
- laser power: 240 W
- absorptivity: 0.45
- material: AlSi10Mg
- hatch distance: 150 um,
- layer thickness (nominal): 30 um
- scan path: bio-directional

- cross section shape: circular

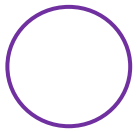

$Q_e(S)$

S: cross section area

Part-scale simulation:

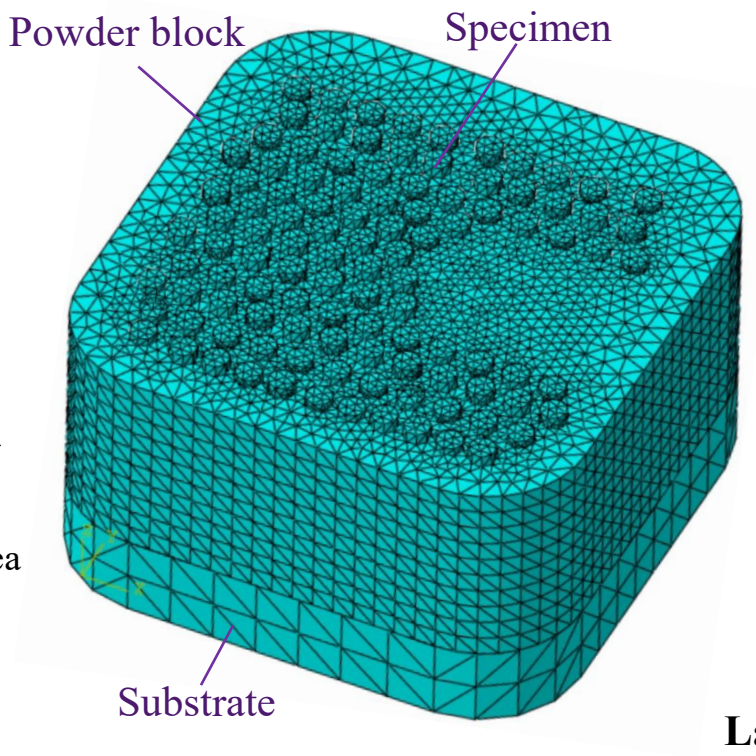

Mesh:

- Total element numbers: 868’364
- Element type: DC3D10

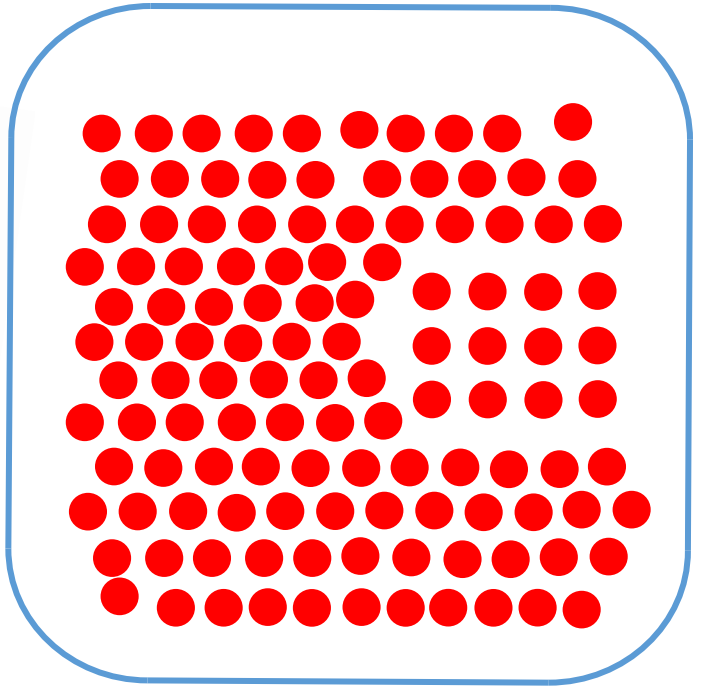

Layer-wise element progressive activation

+

Apply Q_e on **specimen cross sections** ●

[1] Wei L C, Ehrlich L E, Powell-Palm M J, et al., Additive Manufacturing, 2018, 21: 201-208. (0.2-0.3 %)
[2] Jacob G, Donmez A, Slotwinski J, et al., 2016, 27(11): 115601. (84% density)

Temperature results

Temperature evolution during the fabrication procedure

Specimen cluster

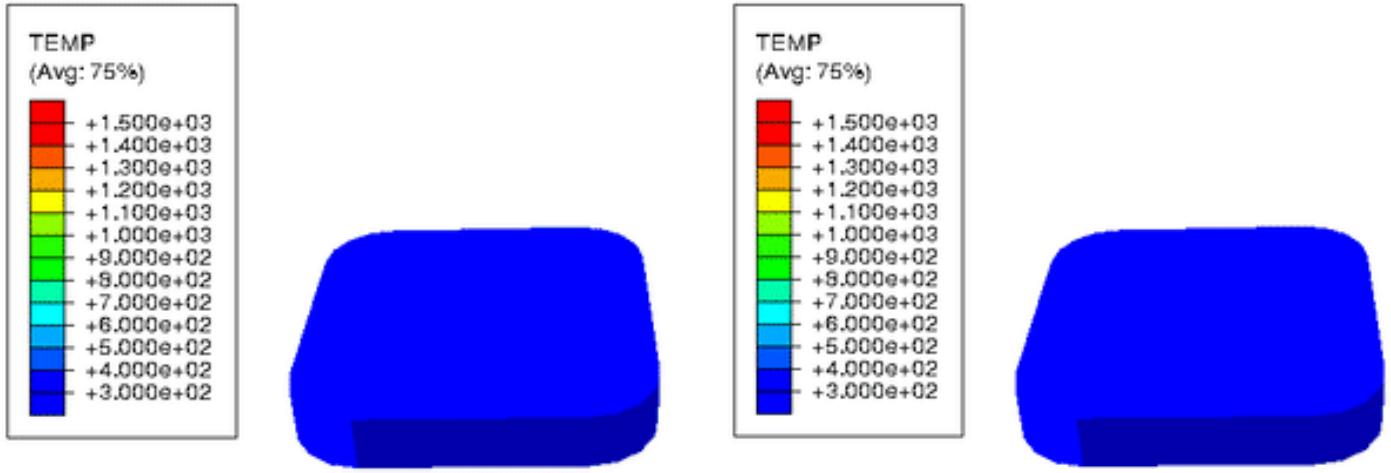

Whole build

Specimen

Computational cost: 20 ~30 mins

Single part

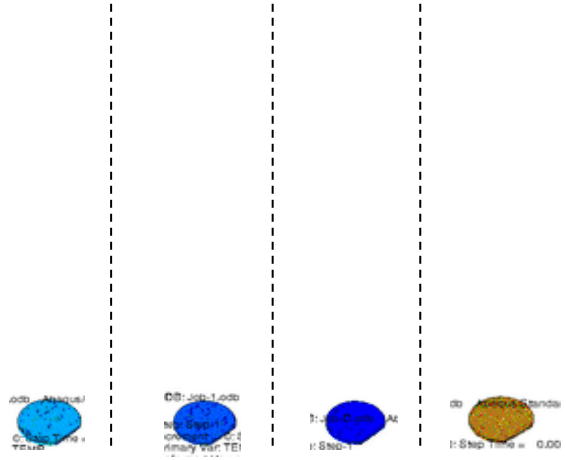

Cross comparison

Computational cost: 5~15 mins

Layer-wise element progressive activation + Layer-wise heat flux attribution

Temperature results

- Temperature field during manufacturing

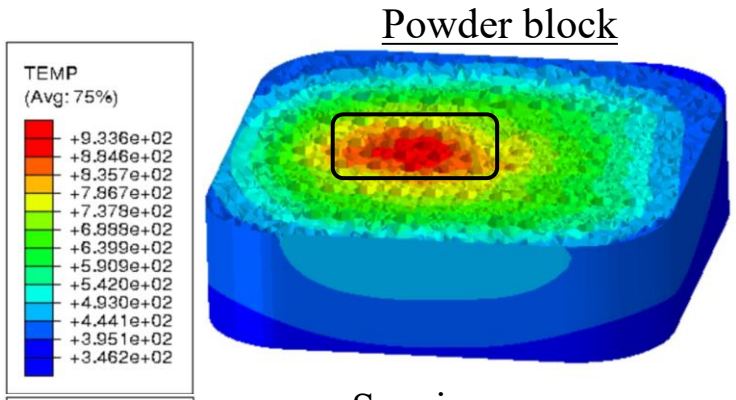

Center region:

- Small cooling rate
- Heat accumulation

⇨ High temperature on the specimen in the center region.

- Temperature distribution after heating (example: Group 4)

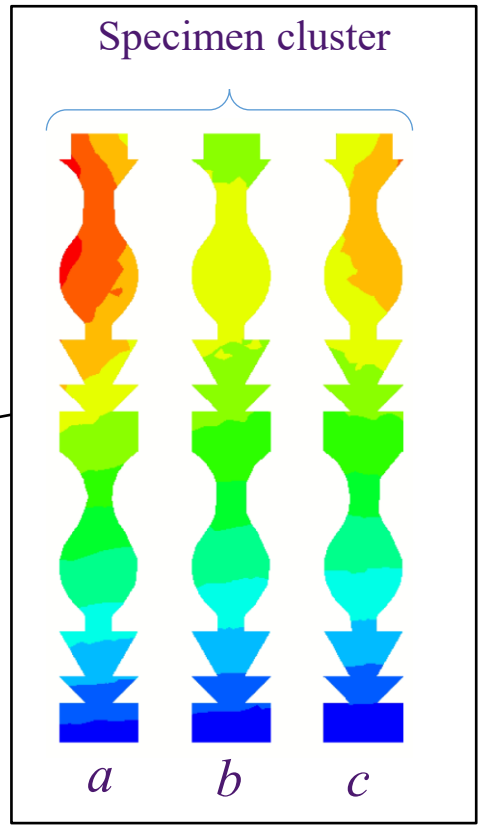

Single part simulation
(for comparison)

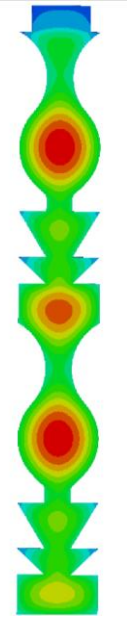

Same geometry
& Thermal load

⇩

Different temperature distribution

Experiment design

Machine: DMG MORI LASERTEC 12 SLM (LT 12 SLM)

Powder: TEKMAT™ AlSi10Mg-63/20-AMS (TEKNA, Montreal, CA)

(by Dominik and Conor)

Lane B, Jacquemetton L, Piltch M, Beckett D. Thermal calibration of commercial melt pool monitoring sensors on a laser powder bed fusion system. NIST Advanced Manufacturing Series 2020;100(35):100-35.

Experiment design

Coaxial photodiode system

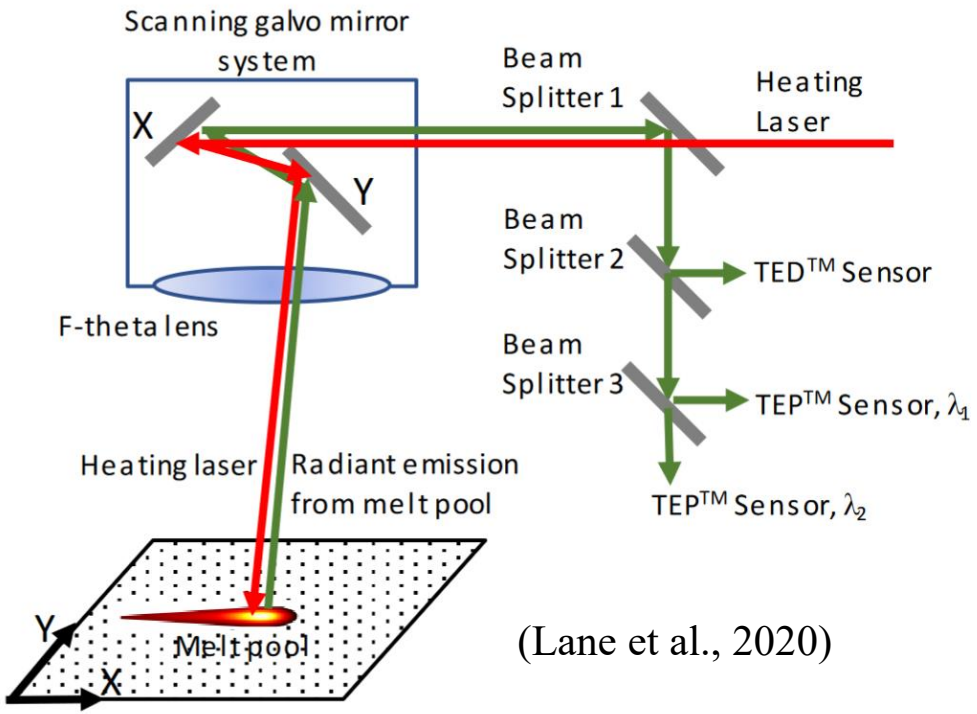

(Lane et al., 2020)

Molten pool temperature measurements (TEP)

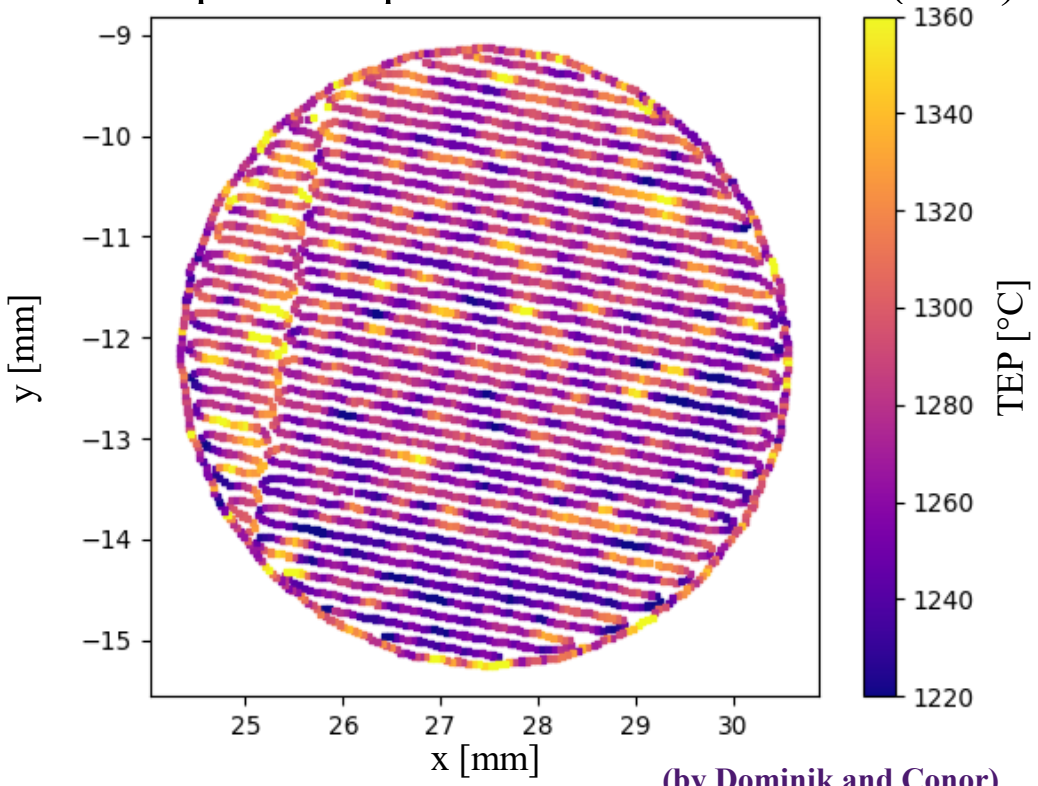

(by Dominik and Conor)

Lane B, Jacquemetton L, Piltch M, Beckett D. Thermal calibration of commercial melt pool monitoring sensors on a laser powder bed fusion system. NIST Advanced Manufacturing Series 2020;100(35):100-35.

Preheating and melt pool temperature relation

Simulation temperature field
Residual temperature after heating
(Preheating of next layer)

VS

Experimental measurement
Average molten pool temperature

(Luo X. et. al.)

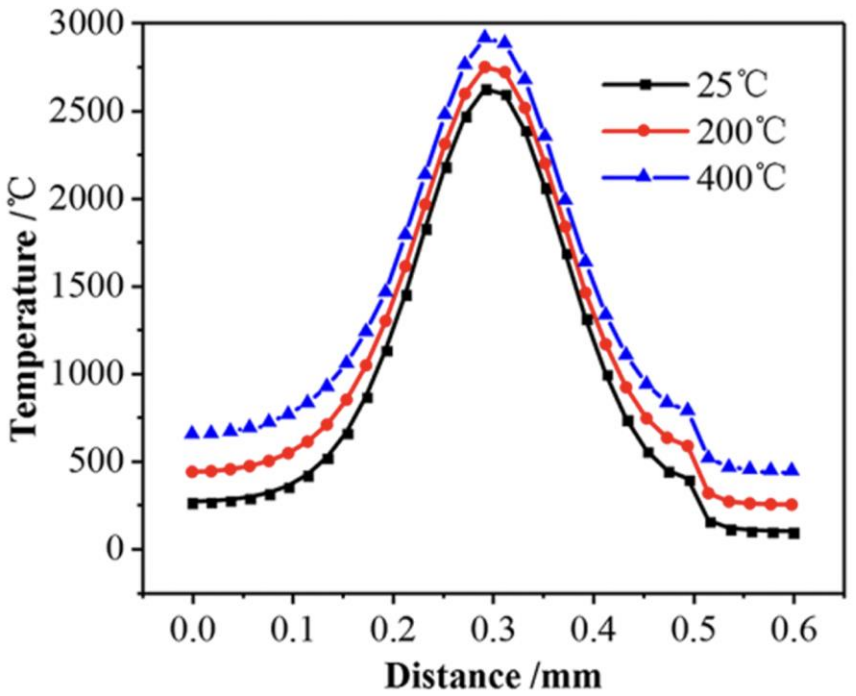

When the **preheating** temperature increases from 25 ℃ to 400 ℃,
the **molten pool central temperature** increases from 2621 ℃ to 2914 ℃.

Luo X, Zhao M, Li J, et al. Numerical study on thermodynamic behavior during selective laser melting of 24CrNiMo alloy steel[J]. Materials, 2019, 13(1): 45.

Measured molten pool temperature

Experimental measurement (by Dominik and Conor)

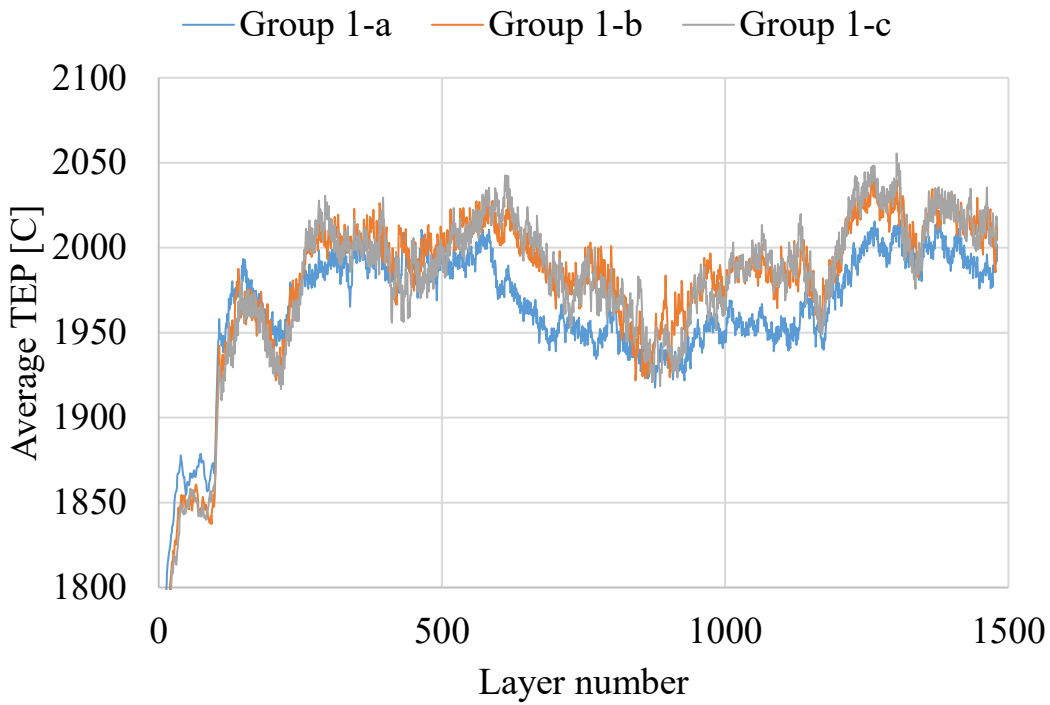

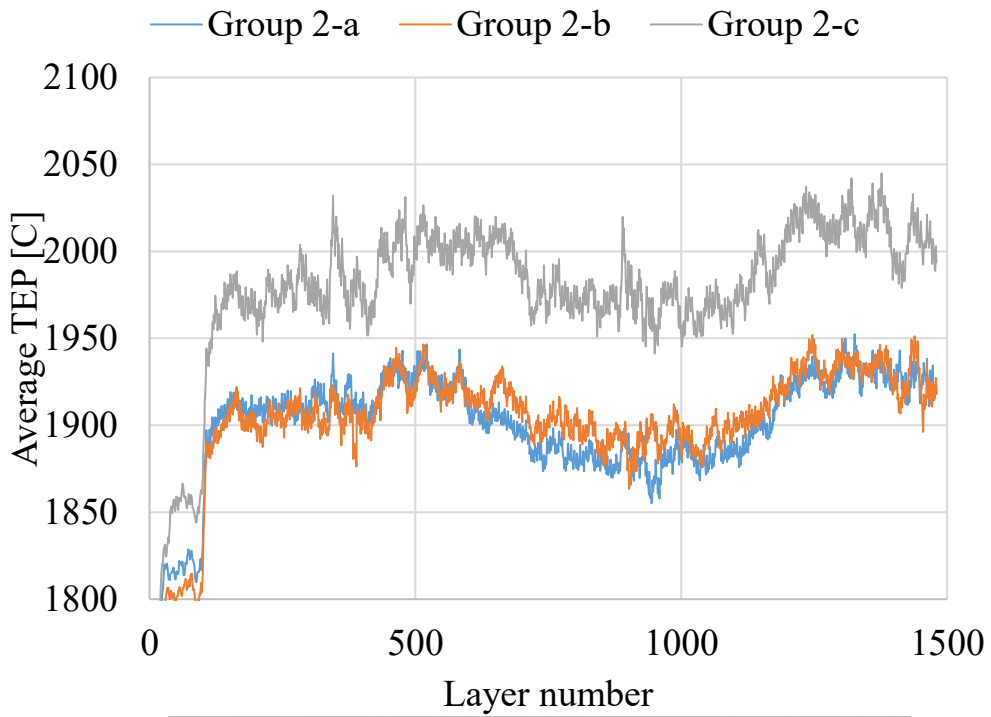

Measured molten pool temperature

Experimental measurement (by Dominik and Conor)

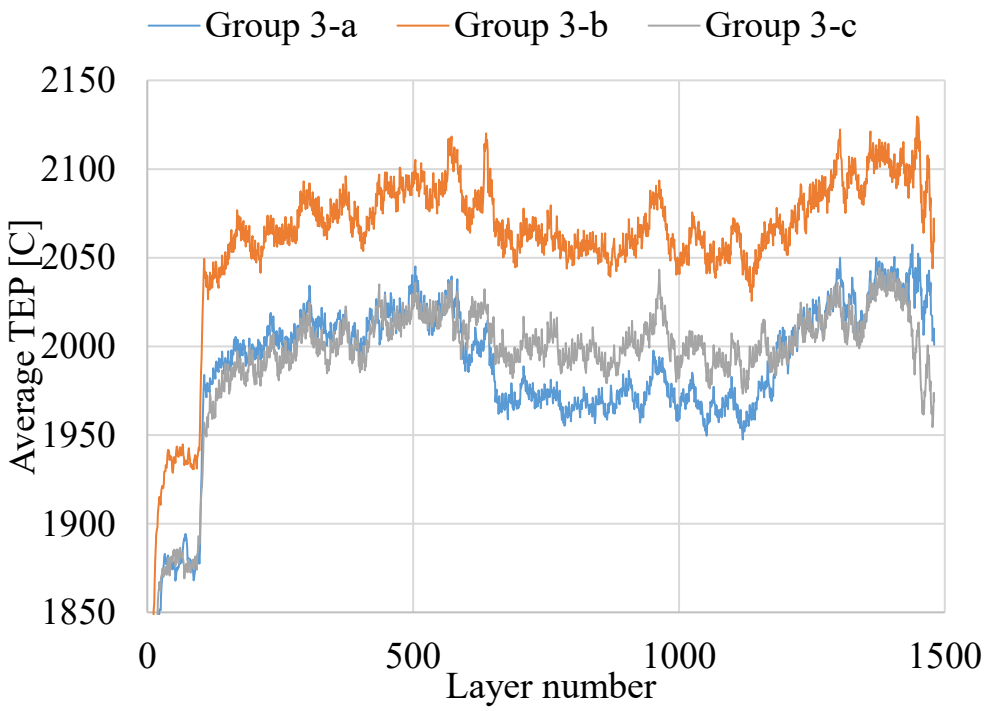

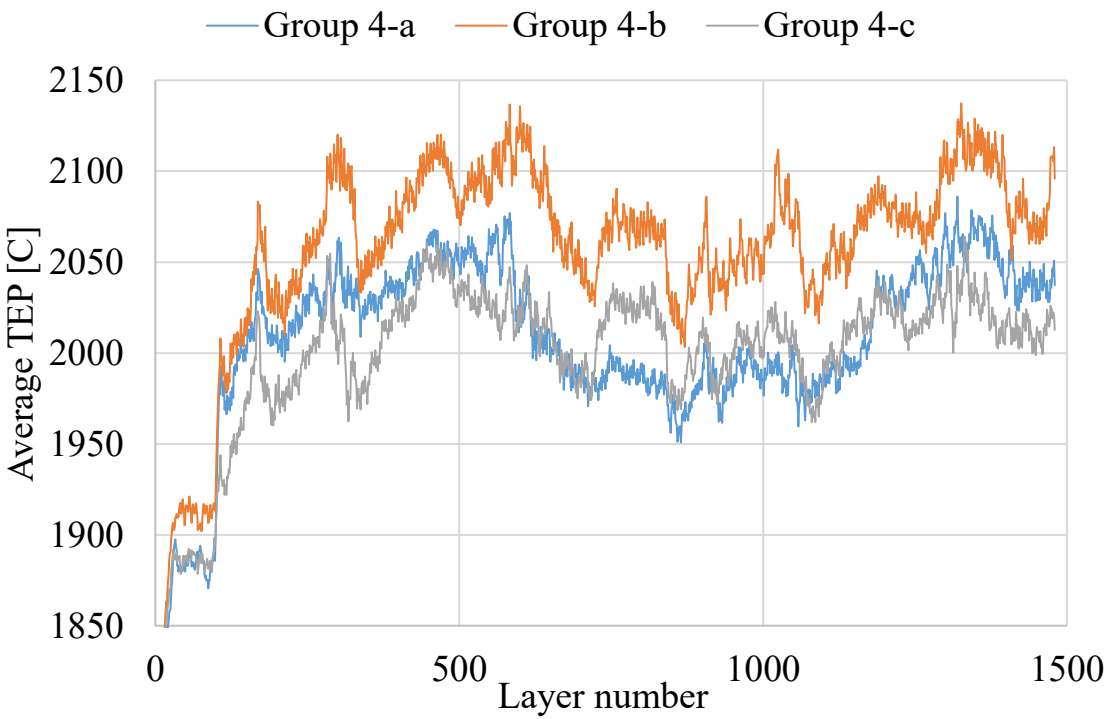

Comparison of simulation and experiment results

Multiple parts simulation VS Experiments

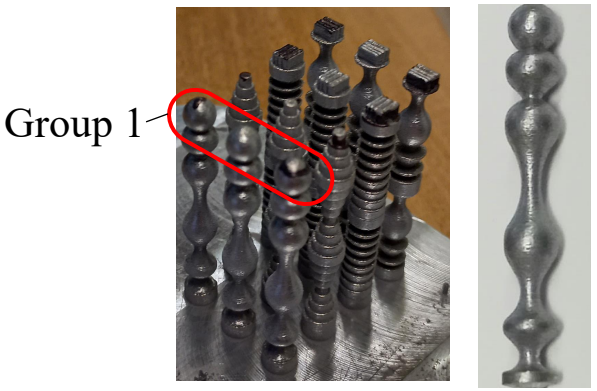

Local fluctuation due to:

- large element size
- large time step
- activation of the new elements
- thermal interactions

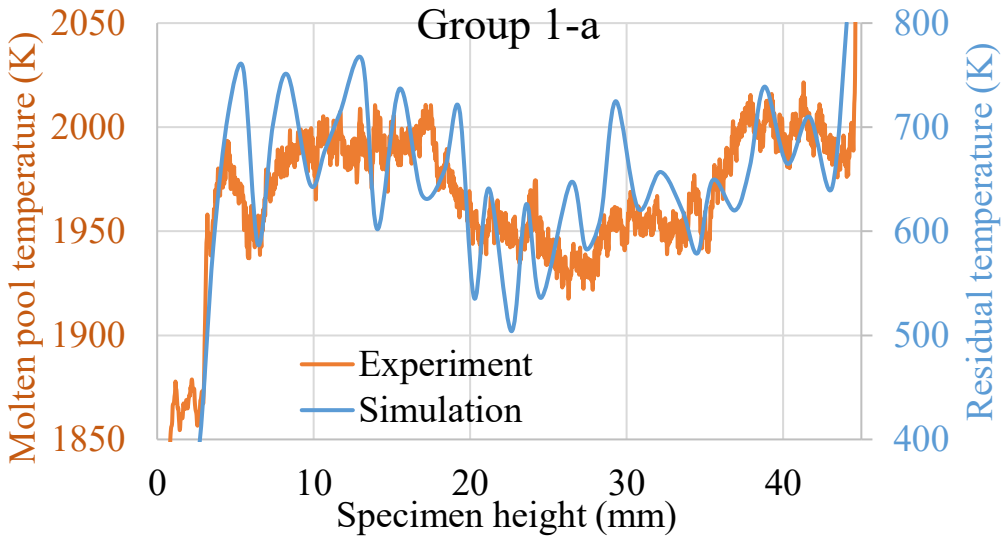

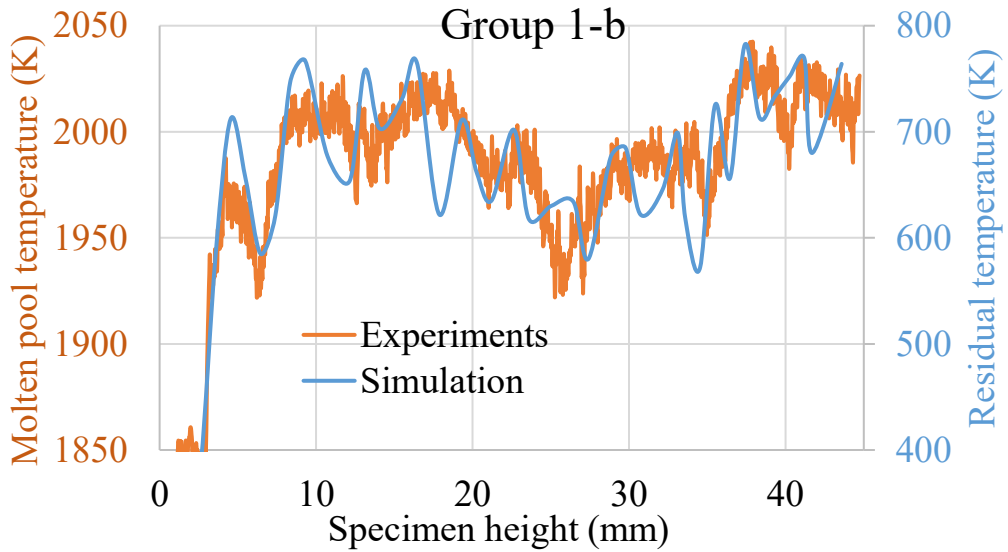

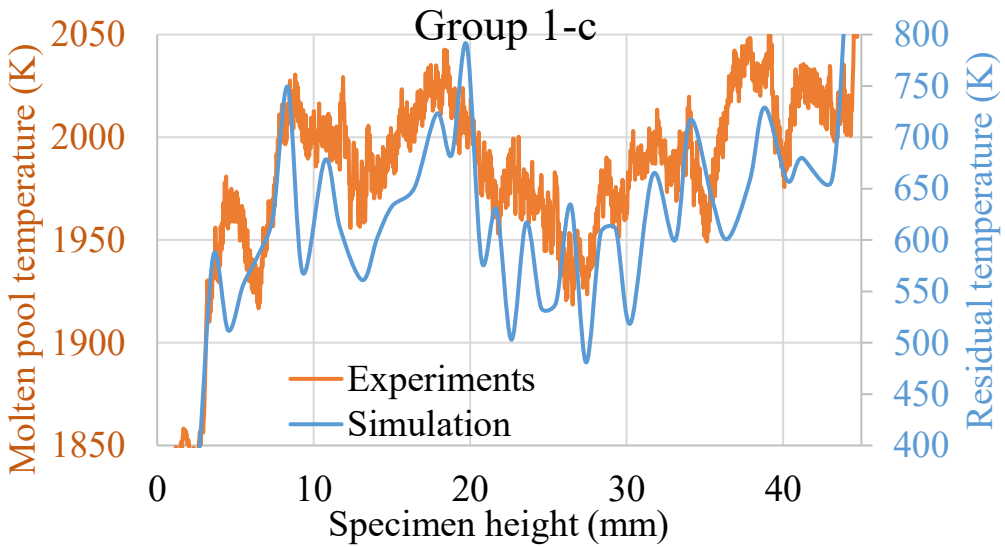

Comparison of simulation and experiment results

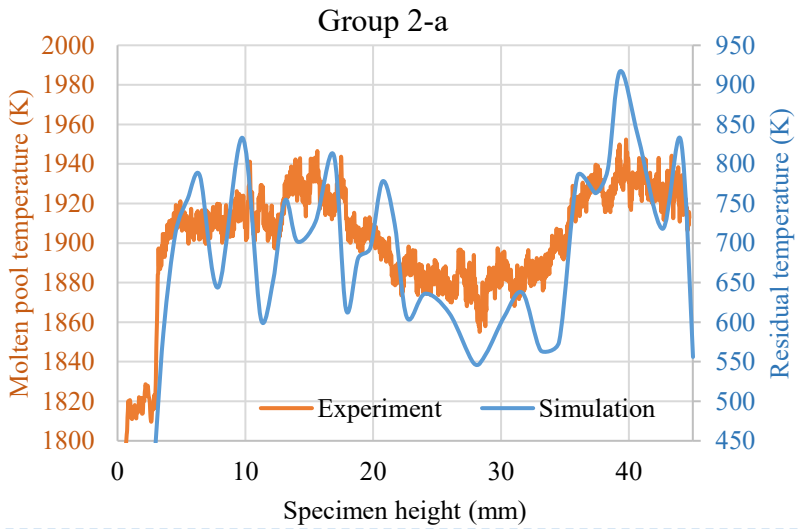

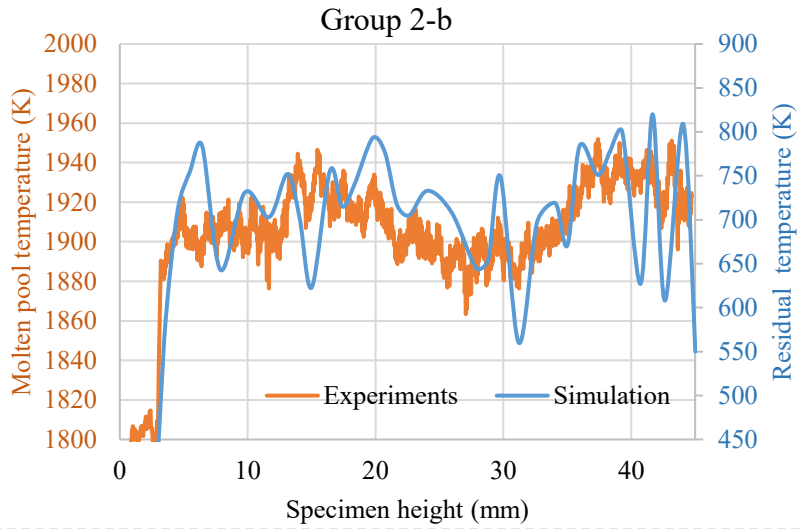

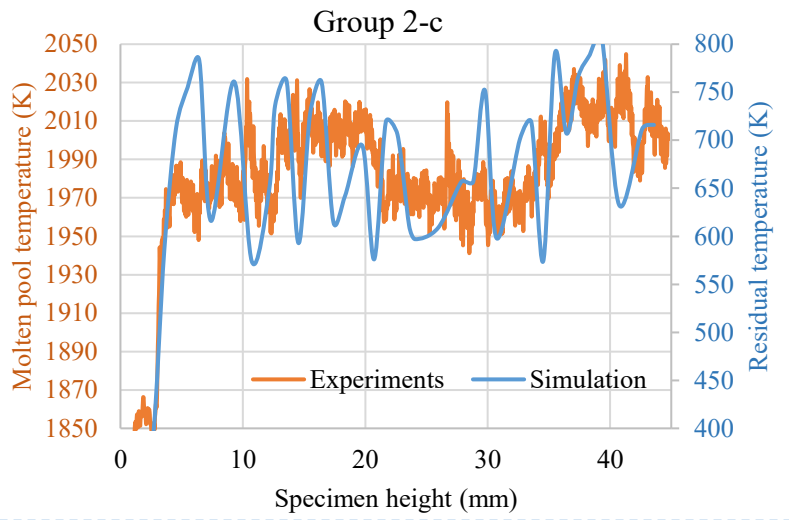

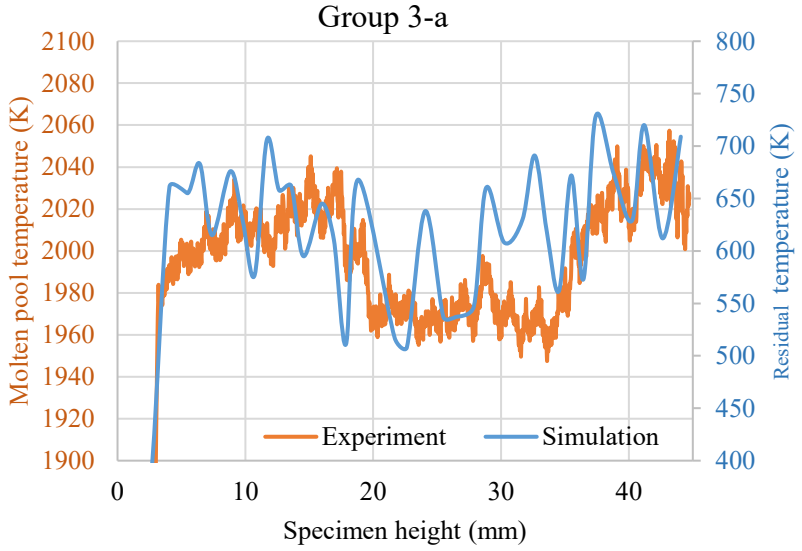

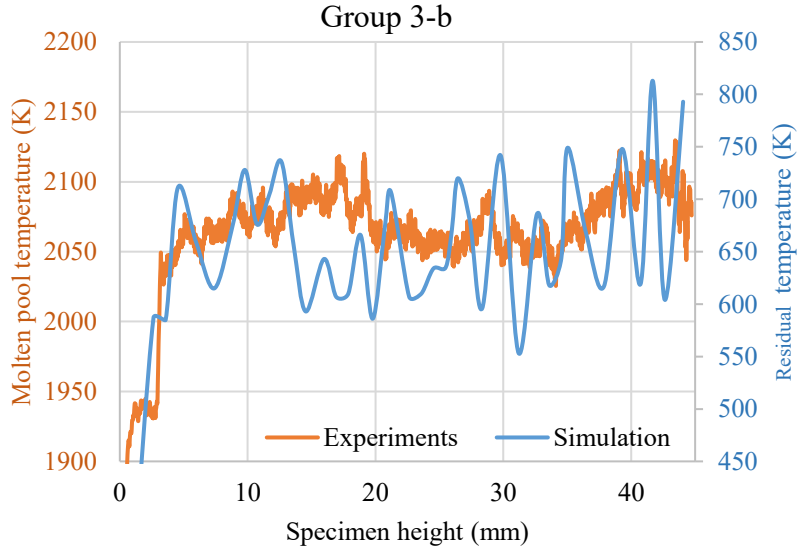

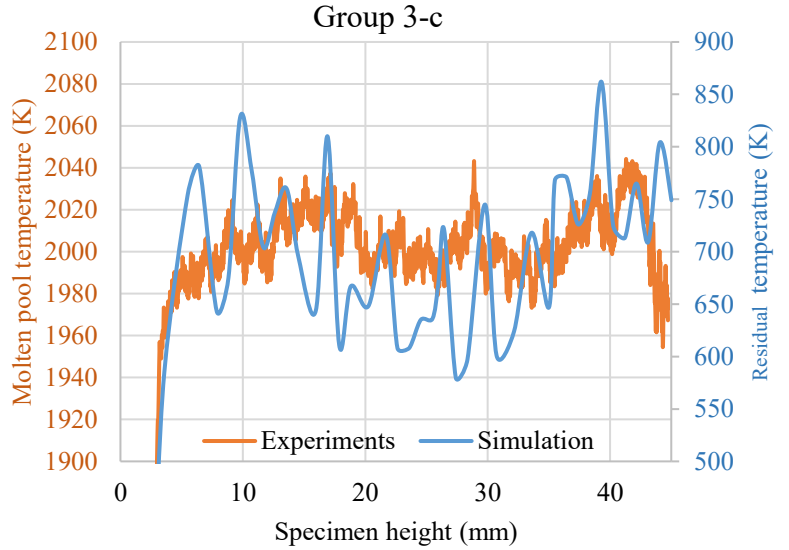

Comparison of simulation and experiment results

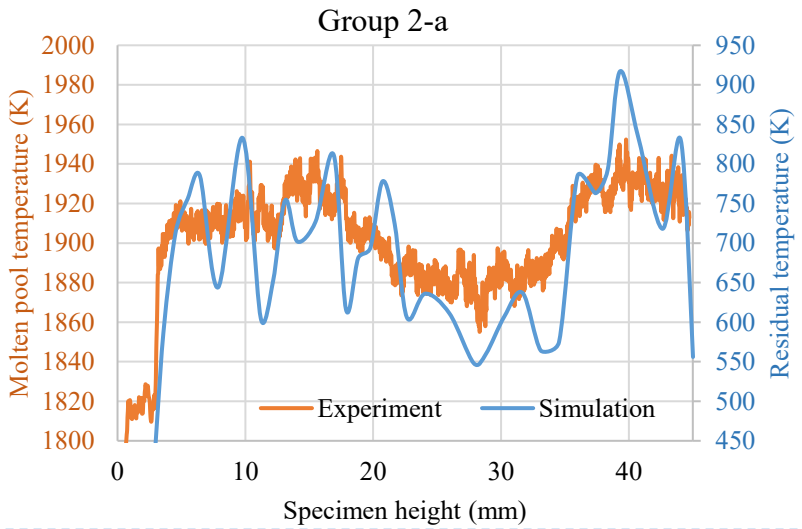

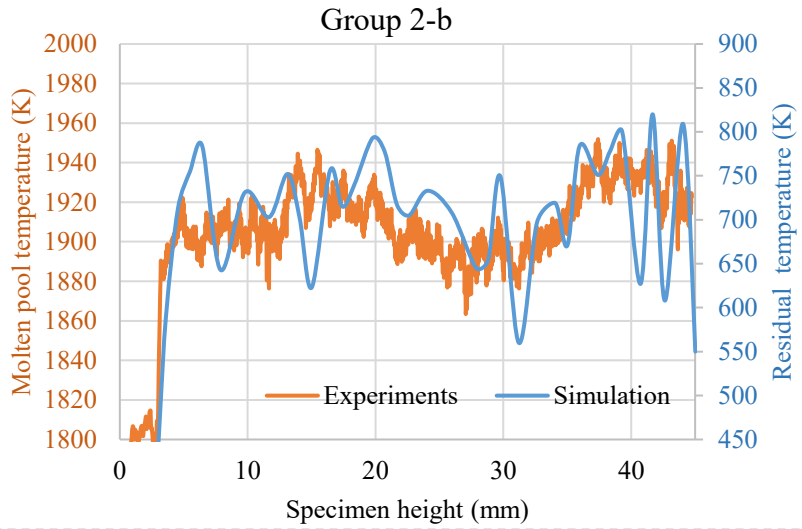

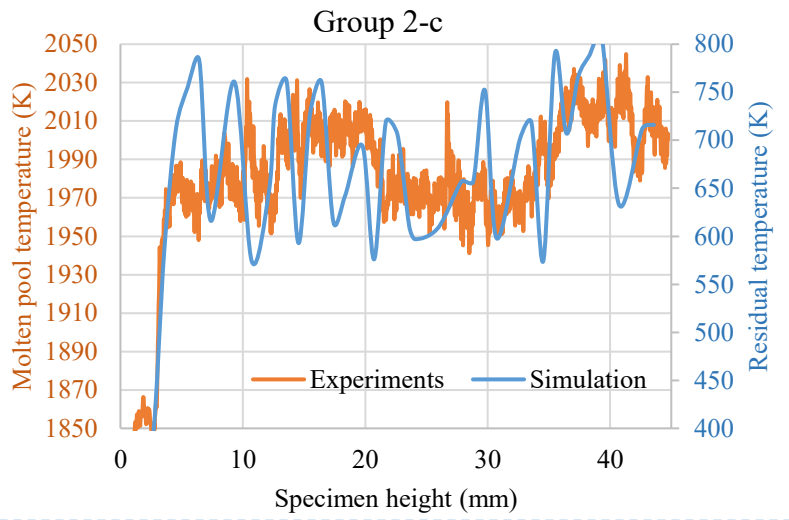

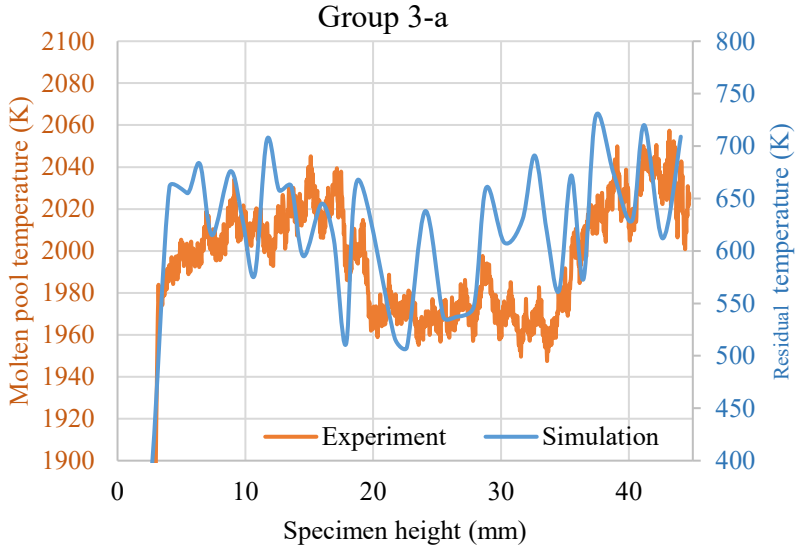

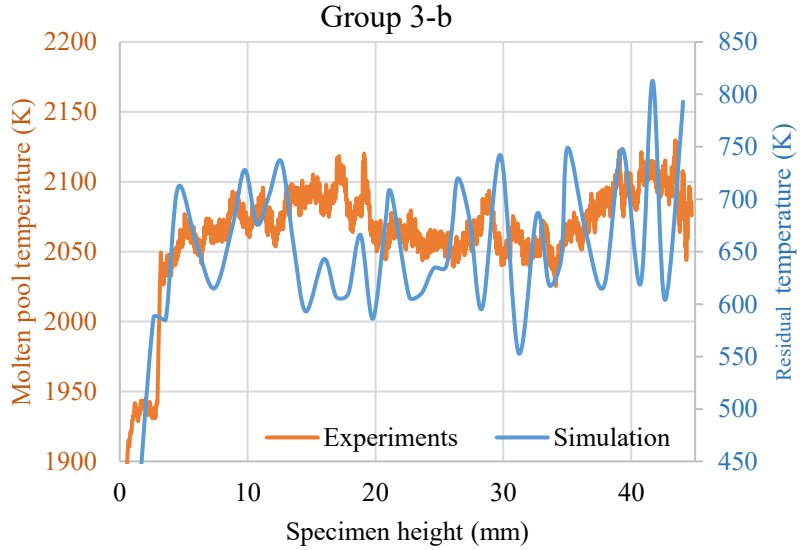

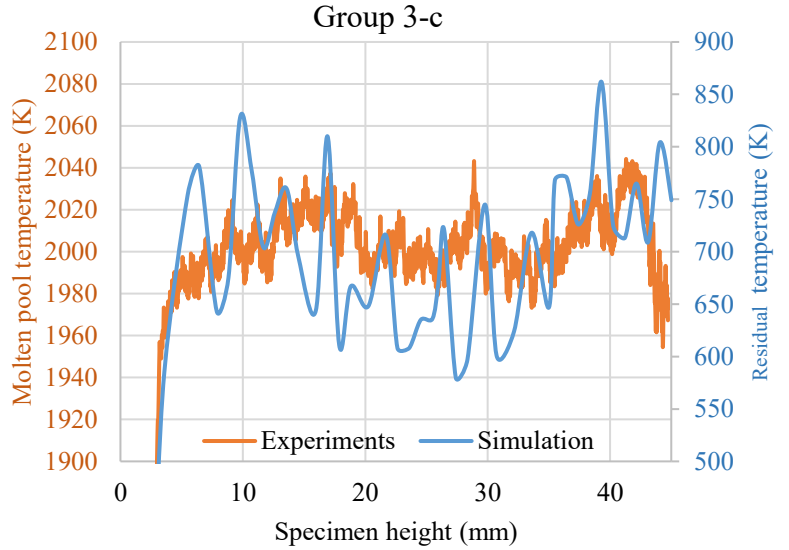

Comparison of simulation and experiment results

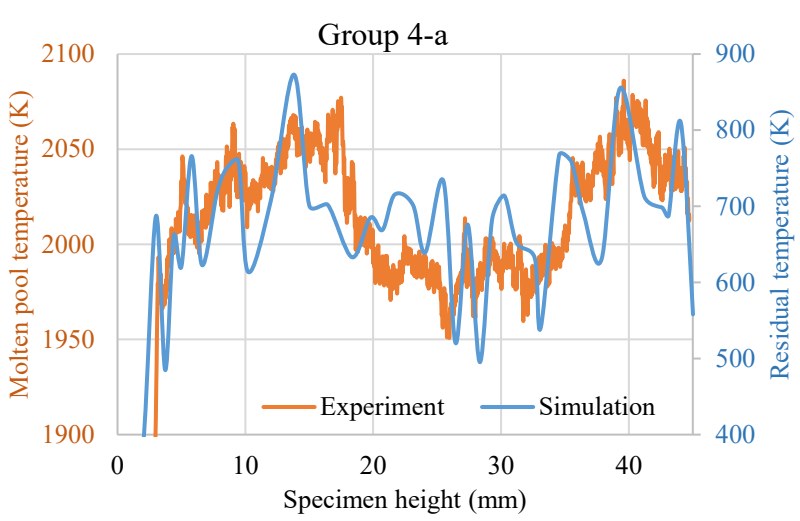

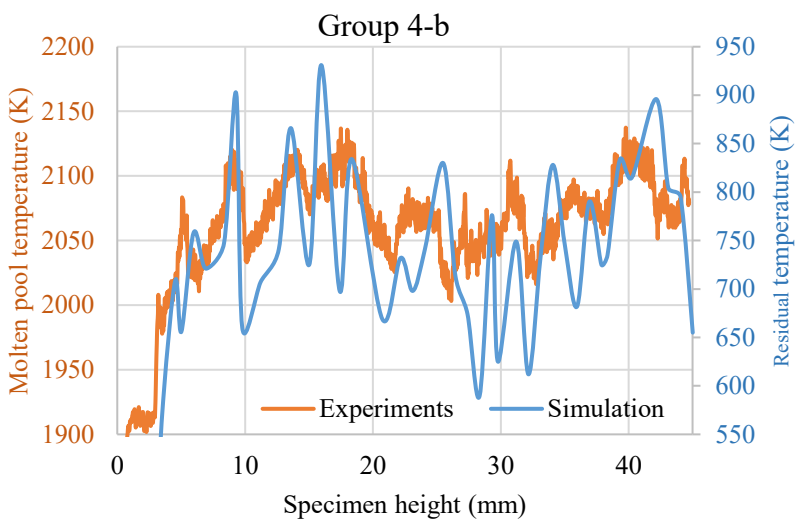

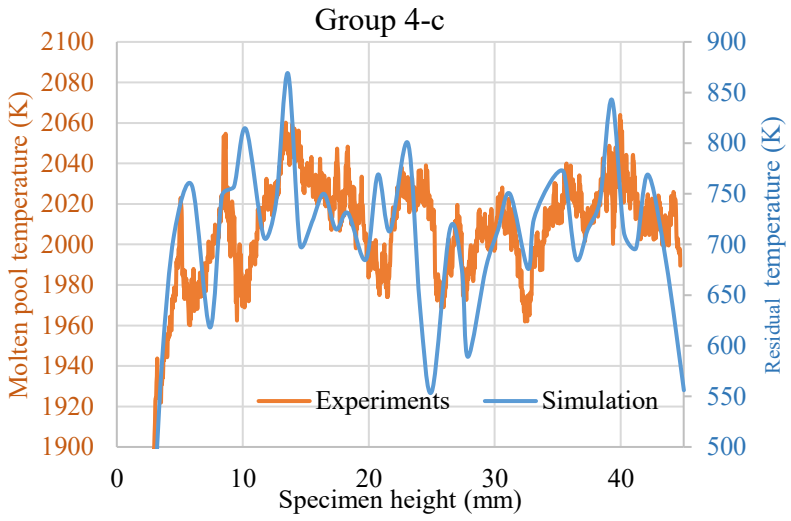

The results indicates:

- the potential relationship between preheating and molten pool temperature;
- the thermal interaction effects by the heat conduction of inter-specimen powders;

Overall, multiple parts simulation and experimental measurement show **a similar trend**.

Comparison of simulation and experiment results

Single part simulation VS **Experiments** (by Dominik)

Simulation (normalized):
Experiment (normalized):

Group 4-a

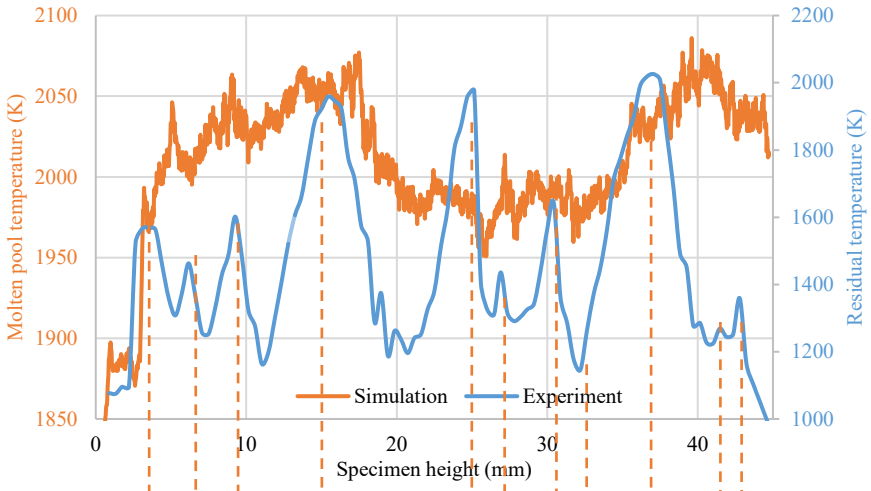

Group 4-b

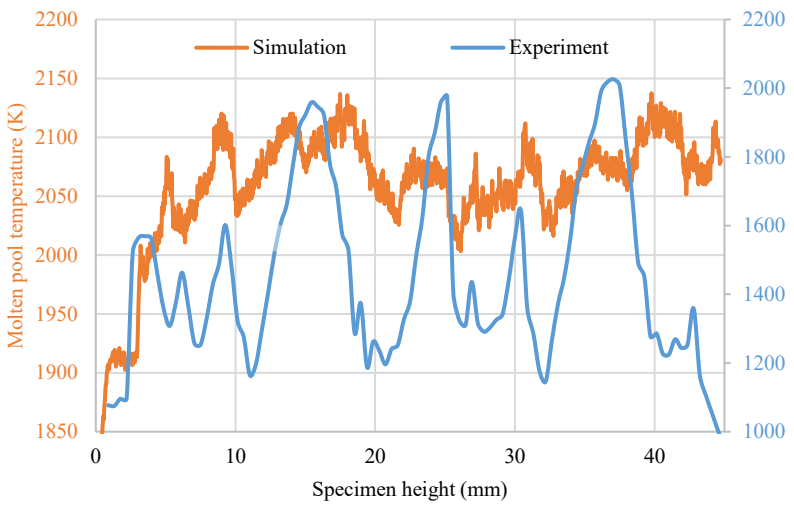

Group 4-c

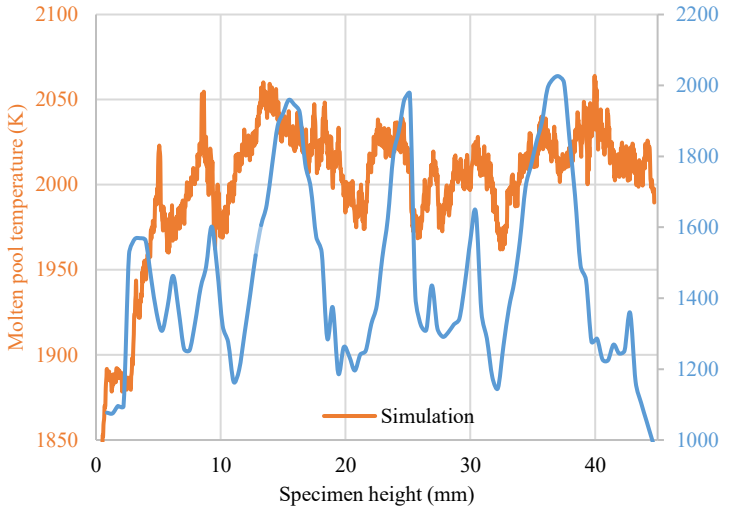

Heat transfer simulation

Experiment specimen

For the **single part** simulation:

- no thermal interaction
- unreasonable thermal boundary conditions

Multiple .vs. single part (Group 4)

Multiple parts

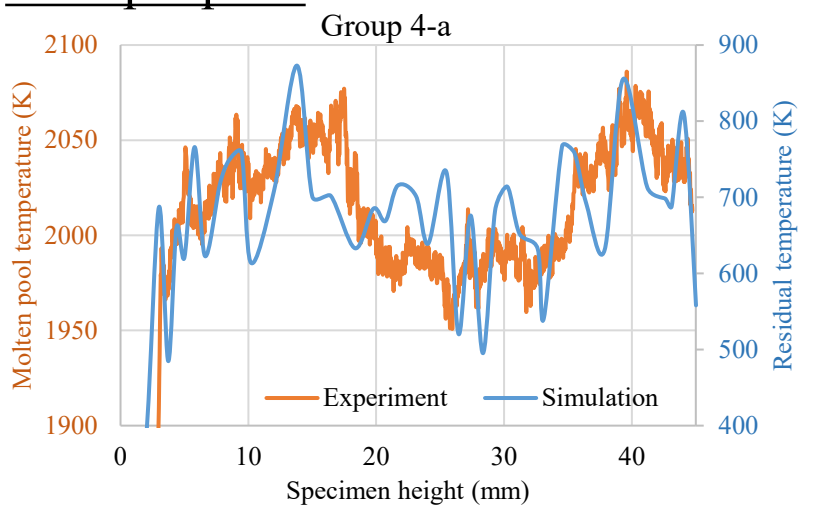

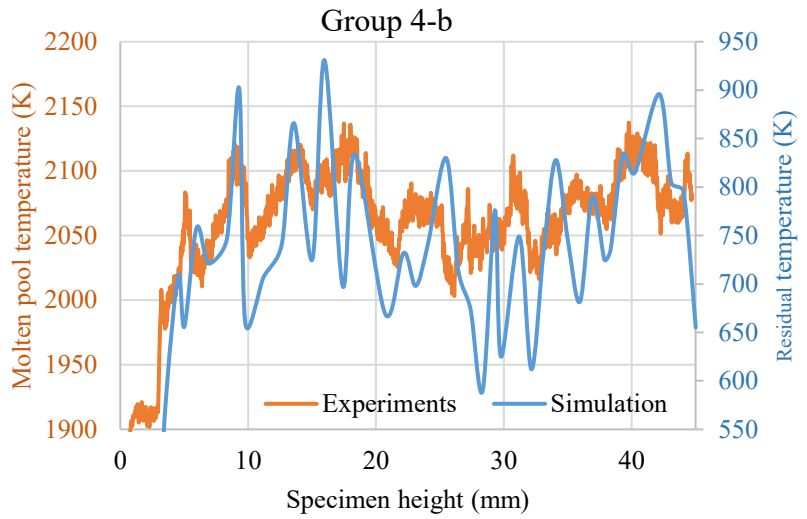

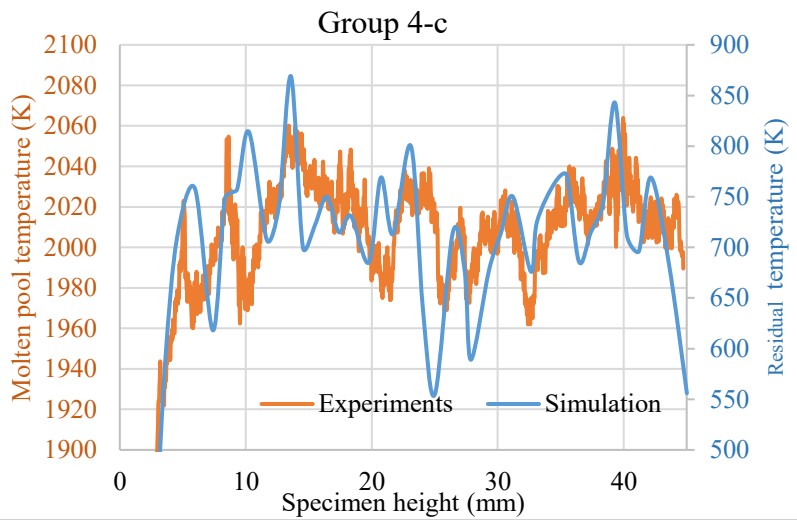

Single parts

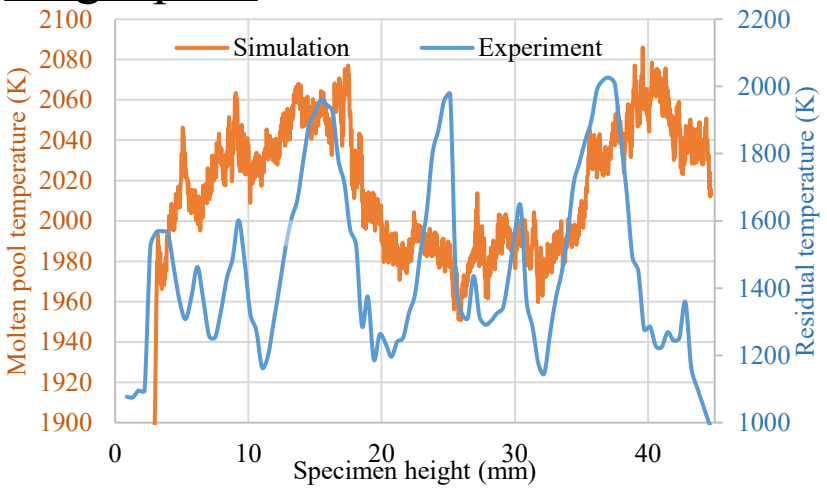

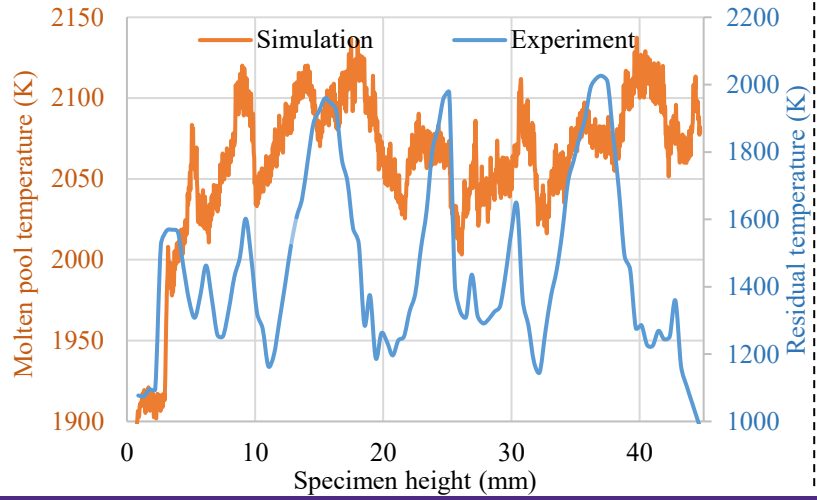

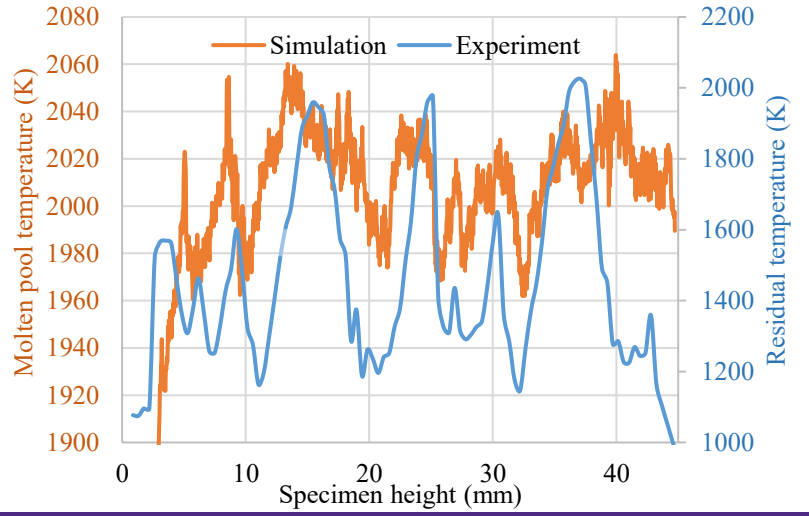

Comparison of simulation and experiment results

Normalization

⇩

R^2 (coefficient of determination)

$$R^2 = 1 - \frac{RSS}{TSS}$$

RSS= sum of squared residuals

TSS= total sum of squares

$$RSS = \sum_i (y_i - f_i)^2$$

$$TSS = \sum_i (y_i - \bar{y})^2$$

R^2 (Multiple parts simulation VS Experiments)

	a	b	c
Group 1	0.48	0.66	0.6
Group 2	0.32	0.43	0.14
Group 3	0.35	-0.76	-0.09
Group 4	0.34	0.53	0.44

R^2 (Single part simulation VS Experiments)

	a	b	c
Group 4	-1.2	-2.59	-3.31

(by Dominik)

$R^2 < 0$: large difference

Feasibility in large-scale thermal modeling

Multiple islands heating test:

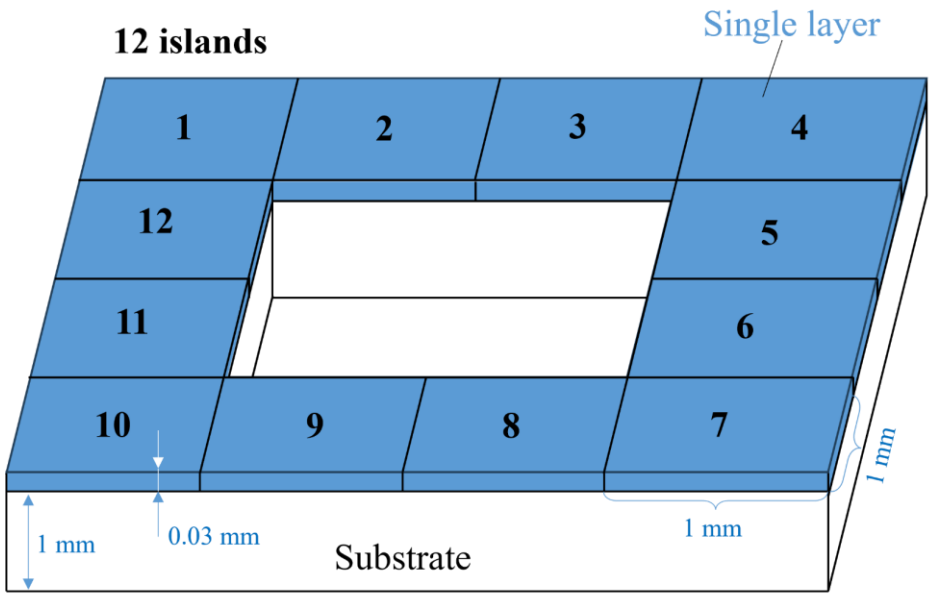

Model geometry

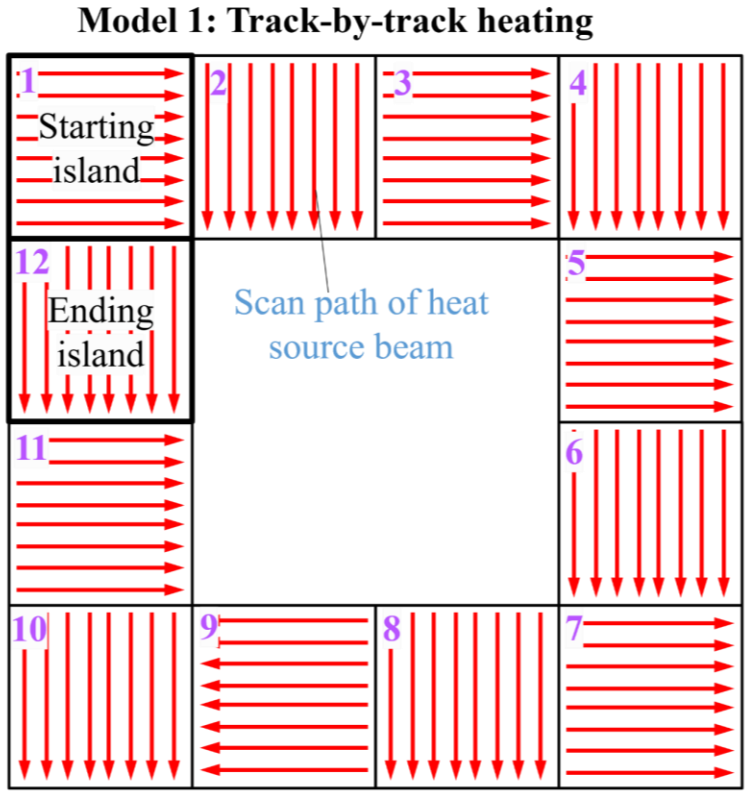

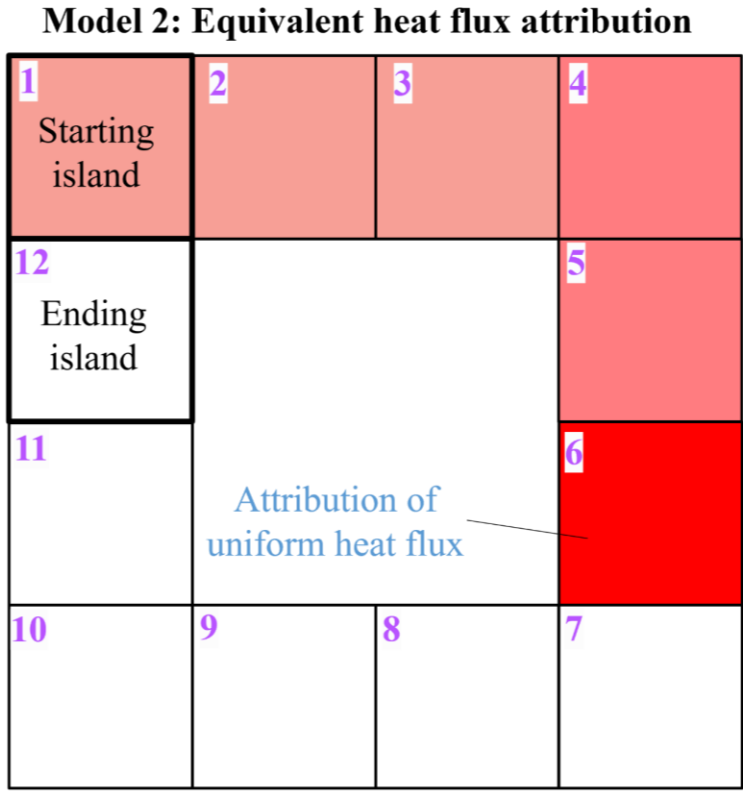

Island deposition sequence: 1-2-3-4-5-6-7-8-9-10-11-12

Two different heating configurations

Feasibility in large-scale thermal modeling

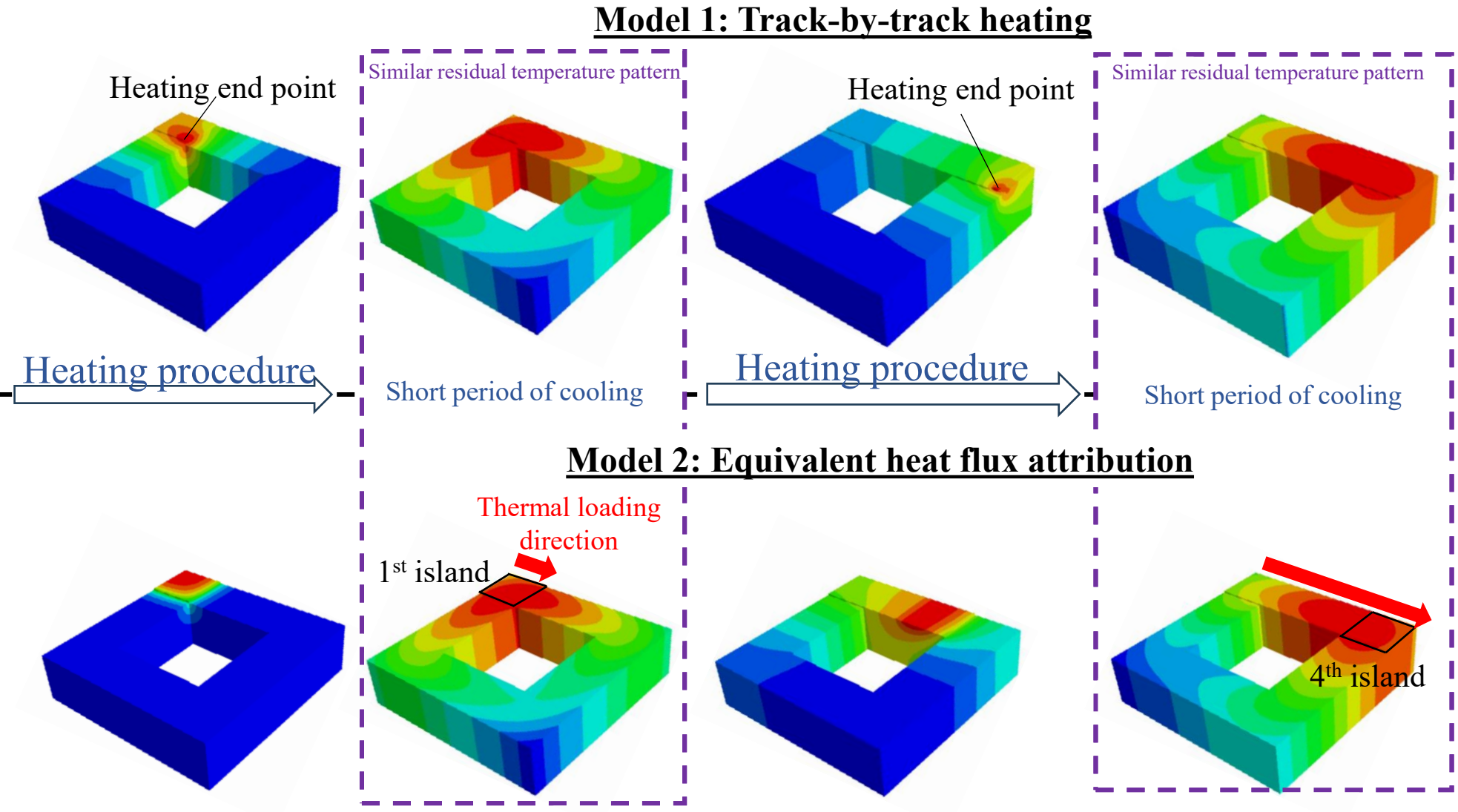

- High thermal conductivity,
- Rapid scan speed,
- Large island area,

Heating by equivalent heat flux attribution always produces a temperature pattern similar to that achieved by track-by-track heating.

Feasibility in large-scale thermal modeling

Model 1: Track-by-track heating

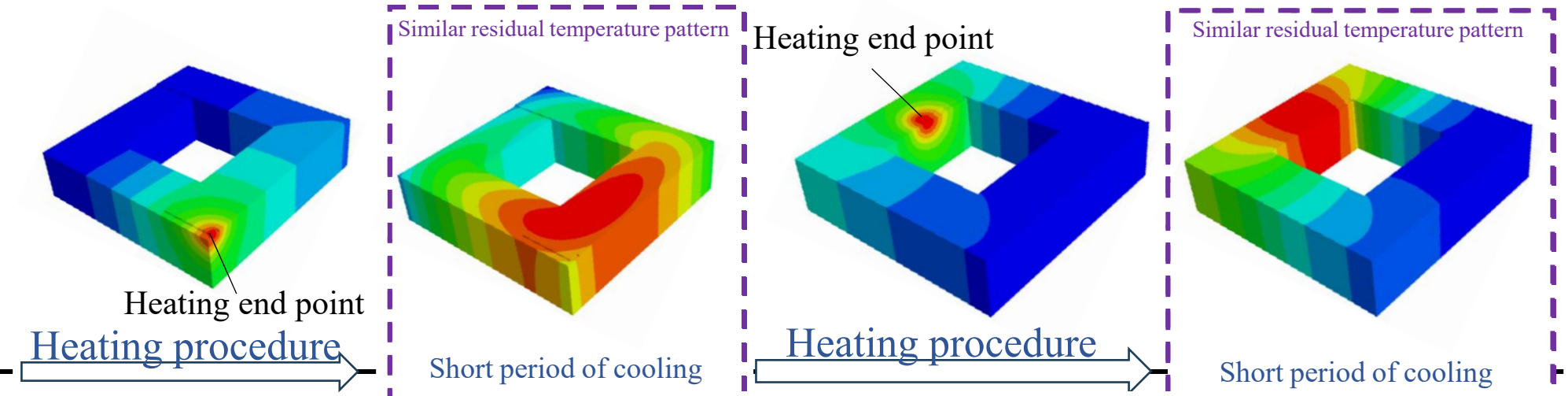

Model 2: Equivalent heat flux attribution

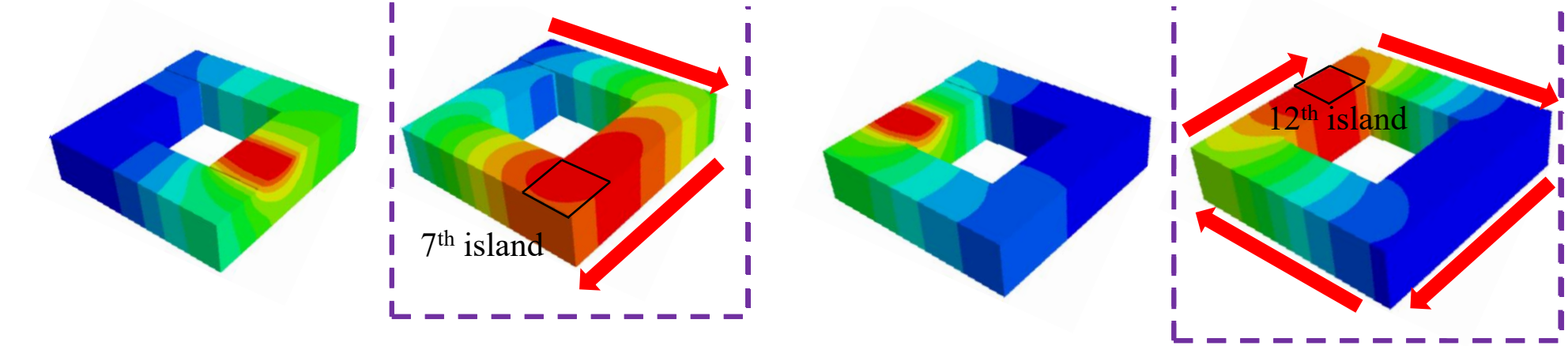

- High thermal conductivity,
- Rapid scan speed,
- Large island area,

Heating by equivalent heat flux attribution always produces a temperature pattern similar to that achieved by track-by-track heating.

Feasibility in large-scale thermal modeling

Strategy 1

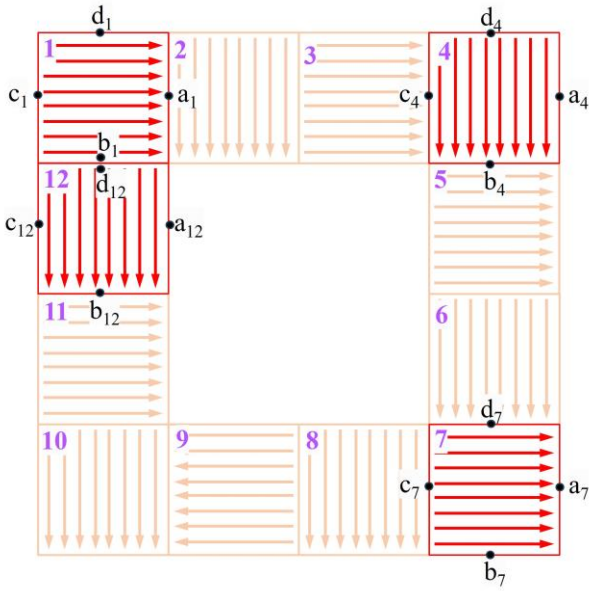

Strategy 2

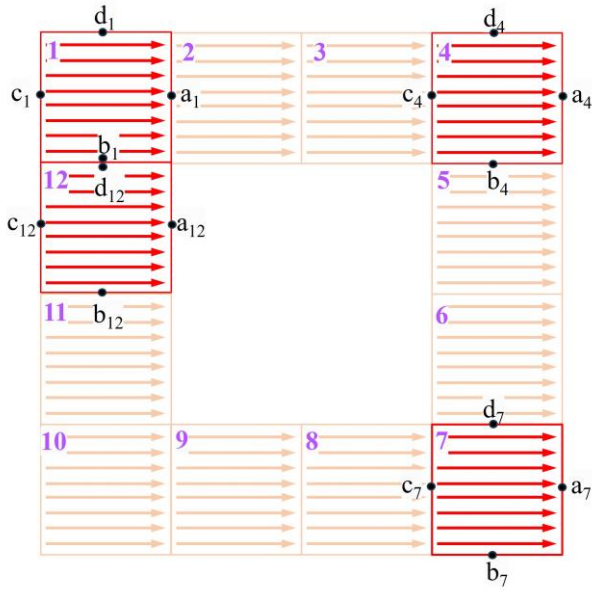

Temperature difference

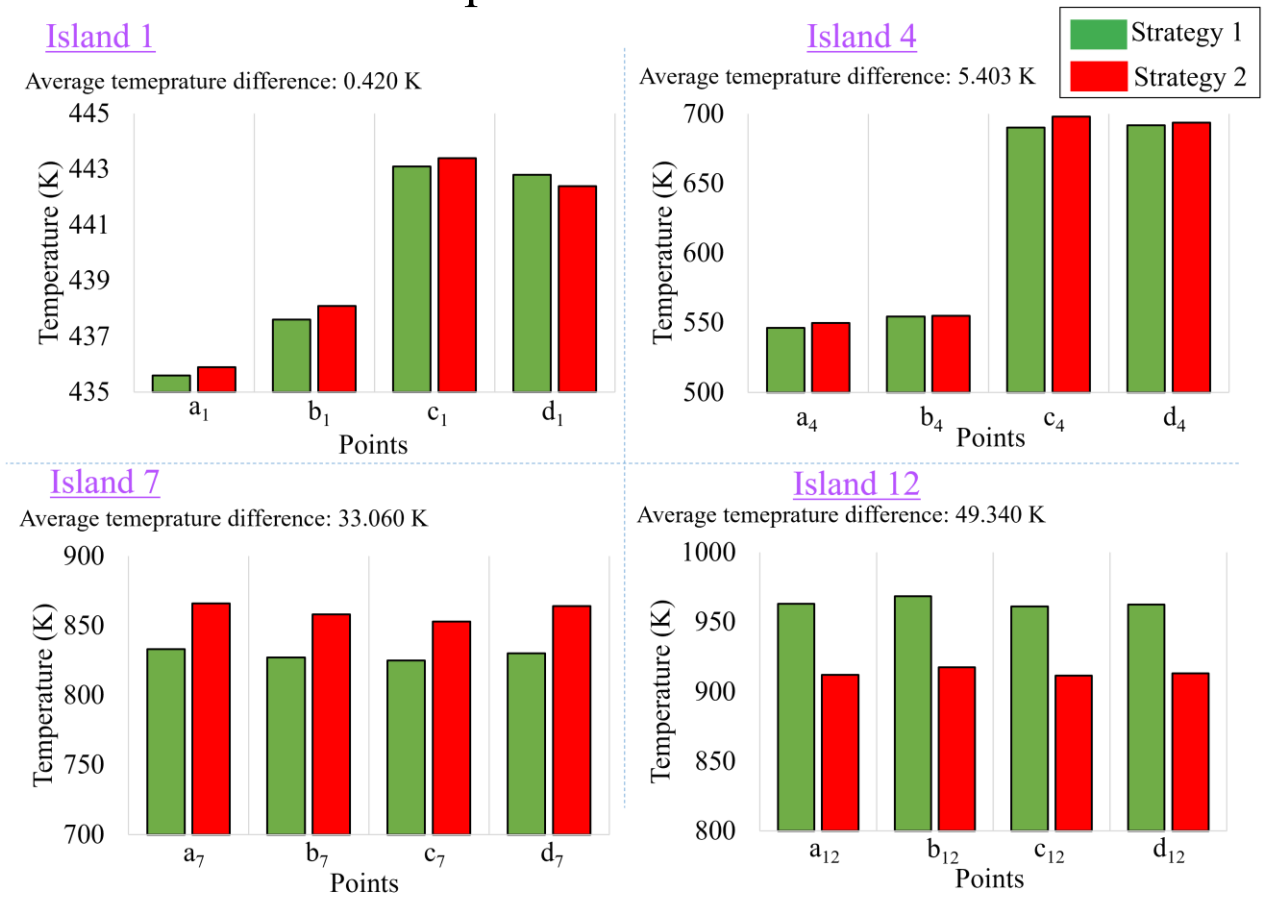

Observations:

1. Scan orientation affects residual temperature pattern;
2. Prediction error can be accumulated with cross-section area
3. Prediction error is tolerable compared to the global temperature change.

Highlights & Summary

- Development of an integrated part-scale modeling framework that combines **layer-wise equivalent heat flux attribution** with **layer-wise element activation**.
- **Justification of the equivalent heat flux** through high-fidelity track-scale simulations.
- **Incorporation of the inter-specimen heat conduction effects** through the powder bed.
- **Remarkable consistency of the simulated temperature data** obtained from each equivalent layer compared to the experimental observations
- A rational explanation for the **different temperature distributions** and cooling rates observed in samples with **identical geometries** but at **different position**.
- A sound physical basis and **excellent computational efficiency**.

Future work

- **Thermal interaction:**

Incorporating depositing sequence for cross sections of different samples;

- **Data-driven approaches:**

Predicting Q_e and temperature curves using machine learning approaches;

- **Different part shape:**

Analyzing the effects of various cross-section shape.

Thank You

Questions?

Northwestern | McCORMICK SCHOOL OF ENGINEERING

Acknowledgements

- Department of Defense Vannevar Bush Faculty Fellowship